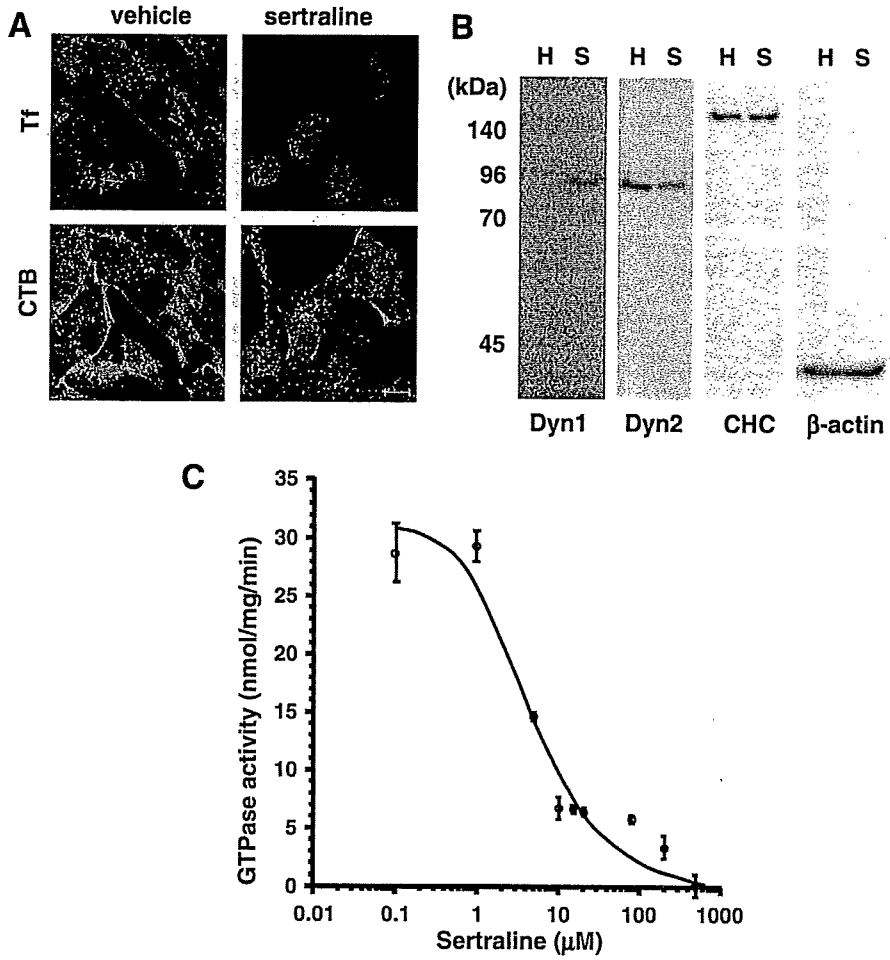


**Fig. 3.** Sertraline inhibits endocytosis in neuronal cultured cells as well as HeLa cells. (A) Inhibition of endocytosis markers by sertraline in SH-Sy5Y cells. Left panels, vehicle; right panels, 20 μM sertraline; upper panels, internalization of Tf (red); lower panels, internalization of CTB (orange). Nuclei were stained with DAPI (blue). Scale bar = 10 μm. (B) Western blotting for endogenous Dyn 1, Dyn 2 and CHC in HeLa (H) and SH-Sy5Y (S) cells. β-Actin was used as an internal control. (C) Sertraline inhibits the GTPase activity of Dyn 2. PS-stimulated GTPase activity of purified Dyn2-$His_6$ (100 nM) was determined in the presence of various concentration of sertraline.

1 was 7.3 ± 1.0 μM [20]. These results suggest that sertraline inhibits Dyn 2 GTPase as well as Dyn 1.

*Effect of sertraline on endocytosis in HeLa and SH-Sy5Y cells*

Dyn 1 K44A, a GTP binding-defective variant [2,16,17], was employed to further examine the mechanism of inhibition of endocytosis by sertraline. We confirmed that purified DynK44A-$His_6$ did not show GTPase activity *in vitro*, as expected (Supplementary Fig. 1). Then, HeLa and SH-Sy5Y cells were transfected with GFP-Dyn1 *wt* or K44A to investigate whether expression of the GTP binding-defective variant would influence endocytosis. Transient transfection of K44A suppressed the internalization of endocytosis markers, while transient transfection of *wt* had no effect (Fig. 4A and B). These findings correspond well with a previous report that the proline-rich domain peptide of Dyn 1 disrupts the interaction between Dyn and amphiphysin and that the PRD peptide of Dyn 1 inhibits Dyn-dependent endocytosis [15]. These results suggest that K44A variant-expressing cells can be used as a negative control of dynamin-dependent endocytosis.

The transfection of Dyn 1 K44A inhibited 83.0 ± 3.2% of Tf uptake (Fig. 4C, column 5 versus 1) and 63.1 ± 6.6% of CTB uptake (Fig. 4C, column 6 versus 2) by HeLa cells. In SH-Sy5Y cells, the corresponding values were 49.2 ± 6.9% of Tf uptake (Fig. 4C, column 9 versus 1) and 22.1 ± 11.2% of CTB uptake (Fig. 4C, column 10 versus 2). In both cell types, Tf uptake was reduced more markedly than CTB uptake (Fig. 4C, column 5 versus 6 and column 9 versus 10). On the other hand, sertraline inhibited 94.8 ± 0.8% of Tf uptake (Fig. 4C, column 7 versus 1) and 50.8 ± 7.7% of CTB uptake (Fig. 4C, column 8 versus 2) in HeLa cells. In SH-Sy5Y cells, the corresponding values were 80.0 ± 3.7% (Fig. 4C, column 11 versus 1) and 35.9 ± 7.5% (Fig. 4C, column 12 versus 2), respectively. The Tf uptake was much more markedly reduced than the CTB uptake in both cell lines (Fig. 4C, column 7 versus 8 and column 11 versus 12). In contrast, the transfection of Dyn 1*wt* did not inhibit Tf or CTB uptake (Fig. 4C, column 3 versus 1, column 4 versus 2).

*Sertraline has little effect on the interaction between PHD of Dyn 1 and PS-liposomes*

SPR analyses were performed to investigate whether sertraline inhibits the interaction between Dyn 1 and PS-liposomes. Dyn-$His_6$ and DynK44A-$His_6$ showed specific interactions with PS-liposomes in the absence of sertraline, unlike DynΔPHD-$His_6$. Moreover, addition of 50 μM sertraline had little effect on the binding of PS-liposomes to either Dyn-$His_6$ or DynK44A-$His_6$ (Supplementary Fig. 2). These results show that the PHD of Dyn 1 is necessary for binding to PS-liposomes and that sertraline does not directly affect the active site of Dyn 1 GTPase.

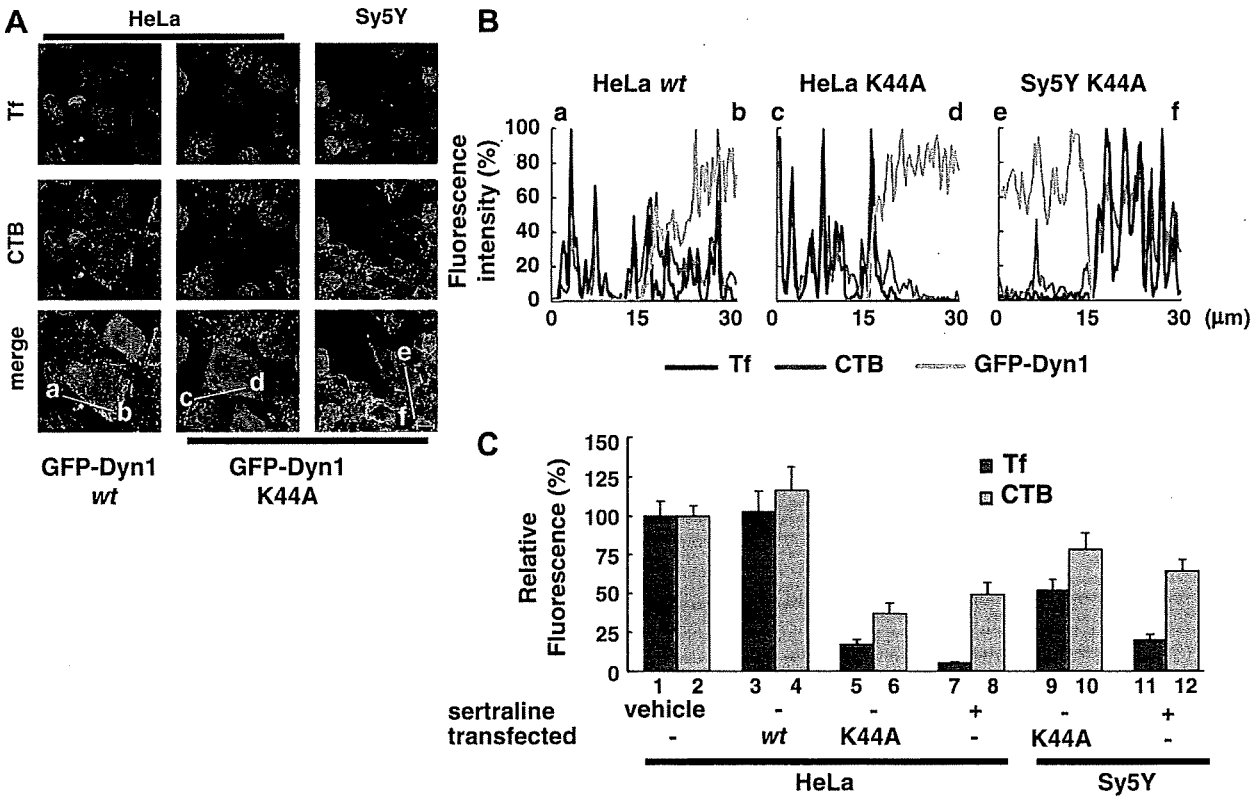


**Fig. 4.** Overexpression of Dyn 1 K44A inhibits internalization of Tf. (A) Endocytosis was inhibited by overexpression of Dyn 1 K44A in HeLa and SH-Sy5Y cells. Left panels, Dyn 1 *wt*-expressing HeLa cells; center panels, Dyn 1 K44A-expressing HeLa cells; right panels, Dyn 1 K44A-expressing SH-Sy5Y cells; Upper panels, internalization of Tf (red); center panels, internalization of CTB (orange); lower panels, GFP-Dyn 1 *wt* or K44A (light green) merged with CTB and Tf. Nuclei were stained with DAPI (blue). Scale bar = 10 μm. (B) Fluorescence intensity of endocytosis markers and GFP-Dyn 1 (*wt* or K44A). Letters (a–f) in both graphs correspond to lines a–b, c–d and e–f in (A). Red line, Tf; orange line, CTB; green line, GFP-Dyn1. (C) Relative fluorescence intensity. Internalized markers was measured with NIH-ImageJ from the images in Figs. 1A, 3A, and 4A (vehicle, $n = 40$; Dyn 1*wt*-expressing HeLa cells, $n = 15$; K44A-expressing HeLa cells, $n = 19$; sertraline-treated HeLa cells, $n = 13$; K44A-expressing SH-Sy5Y cells, $n = 12$; sertraline-treated SH-Sy5Y cells, $n = 10$). Relative fluorescence intensity was calculated in arbitrary units, based on the value for column 1 or 2 (vehicle) as 100%. Red and orange columns show Tf and CTB uptake, respectively, in terms of relative fluorescence intensity. Error bars indicate SEM.

## Discussion

We previously reported that Dyn 1 GTPase activity is inhibited by sertraline *in vitro* [20]. PS-liposomes were used instead of plasma membrane, and membrane protein was not employed in our previous GTPase assay. Here, we examined the effect of sertraline on Tf and CTB uptake in cultured cells. It has been reported that Tf is internalized by receptor-mediated, clathrin- and Dyn-dependent endocytosis [17,27,28]. It is known that the endocytic pathway of CTB involves lipid-raft-dependent internalization *via* glycosphingolipid binding [29]. In this study, internalization of Tf was blocked by 20 μM sertraline in HeLa cells (Fig. 1A and B) and SH-Sy5Y cells (Fig. 3A). Accordingly, we concluded that sertralin may act as an inhibitor of Dyn-dependent endocytosis in both neuronal and non-neuronal cultured cells.

In our previous study, only Dyn 1 was employed for *in vitro* GTPase assay. Thus, it remained unknown whether sertraline inhibits other Dyn isoforms. Here, we found that sertraline inhibited endocytosis in HeLa cells (Fig. 1), which contain Dyn 2, but lack endogenous Dyn 1 (Fig. 3B). Furthermore, sertraline inhibited Dyn 2 GTPase activity *in vitro* (Fig. 3C). These results indicate that sertraline inhibited Dyn 2 GTPase in HeLa cells. Thus, our results indicate that sertraline suppresses Dyn-dependent endocytosis *via* inhibition of both Dyn 1 and Dyn 2 GTPase activities. Moreover, inhibition of Tf uptake by sertraline in HeLa cells was different from that in SH-Sy5Y cells (Fig. 4C, columns 7 versus 11). This difference may be a consequence of the difference in expression of Dyn isoforms between the two cell lines.

Sertraline inhibited Tf uptake within 5 min (Fig. 2A). The inhibition lasted for more than 60 min (Fig. 2A) and could be reversed by washing the cells (Fig. 2C). These results indicate that sertraline is a rapid, continuous and reversible inhibitor of Dyn-dependent endocytosis of Tf in HeLa cells. In this study, SPR analysis showed that sertraline had little effect on the interaction between the PHD of Dyn 1 and PS-liposomes (Supplementary Fig. 2). The results of SPR analysis are consistent with our previous finding that sertraline is not a competitive inhibitor with respect to PS-liposomes [20]. Sertraline is not a long-chain compound, and therefore is not expected to interfere with liposome formation or to disrupt the membrane structure of cultured cells.

It is known that Dyn 1 K44A is a variant deficient in GTP binding [2,16,17]. There are two possible pathways through which Dyn 1 K44A expression may cause inhibition of endocytosis. First, Dyn 1 K44A has the *PXXP* motif, like Dyn 1 *wt*, at the C-terminus. It is well known that the *PXXP* motif of Dyn 1 interacts with SH3 domain-containing proteins such as amphiphysin [13]. Hence, Dyn 1 K44A may compete with endogenous Dyn for binding to SH3 domain-containing proteins *in vivo* [15]. Second, Dyn 1 K44A showed no GTPase activity *in vitro* (Supplementary Fig. 1), in agreement with several previous reports [2,16,17]. Moreover, it was reported that tetramerization of Dyn is necessary for GTPase activity [12]. Therefore, Dyn 1 K44A may act as an inhibitor of endocytosis by forming inactive tetramers with Dyn 1 *wt* [10]. The transfection of Dyn 1 K44A indeed reduced Tf uptake in HeLa and SH-Sy5Y cells, respectively, but sertraline resulted in greater reductions of Tf uptake (Fig. 4C). These differences between the effects of Dyn 1 K44A

transfection and sertraline on internalization of Tf and CTB indicate that different mechanisms of inhibition of endocytosis are involved.

Although citalopram is a SSRI, like sertraline [21,26], it did not inhibit the uptake of Tf or CTB (Fig. 1A and B). This result may be consistent with the previous finding that citalopram did not influence the regulation of norepinephrine [30]. The uptake of Tf was more markedly reduced by sertraline than by CPZ, whereas sertraline inhibited the uptake of CTB as effectively as did CPZ in HeLa cells (Fig. 1B). It is well known that CPZ is a clathrin-dependent endocytosis inhibitor [25]. The difference between sertraline and CPZ in the inhibition of Tf uptake is consistent with our previous report that the $IC_{50}$ values of sertraline and CPZ for Dyn 1 GTPase were 7.3 ± 1.0 and 47.2 ± 23.1 μM, respectively [20]. Thus, it might appear that the difference between inhibition of Tf uptake by sertraline and CPZ can be attributed to the difference of inhibitory potency towards Dyn 1 GTPase. In conclusion, this report presents evidence that sertraline suppresses endocytosis in cultured cells.

## Acknowledgments

This work was supported in part by Grants-in-Aid for Scientific Research from the Ministry of Education, Science, Sports and Culture of Japan (to K.T. and H.M.). The authors thank Ms. Shigemi Terakubo and Ms. Satomi Yamazaki for their technical assistance.

## Appendix A. Supplementary data

Supplementary data associated with this article can be found, in the online version, at doi:10.1016/j.bbrc.2009.11.067.

## References

[1] J.R. Henley, E.W. Krueger, B.J. Oswald, M.A. McNiven, Dynamin-mediated internalization of caveolae, J. Cell Biol. 141 (1998) 85–99.
[2] H. Damke, T. Baba, D.E. Warnock, S.L. Schmid, Induction of mutant dynamin specifically blocks endocytic coated vesicle formation, J. Cell Biol. 127 (1994) 915–934.
[3] J.A. Mears, P. Ray, J.E. Hinshaw, A corkscrew model for dynamin constriction, Structure 15 (2007) 1190–1202.
[4] S.M. Ferguson, G. Brasnjo, M. Hayashi, M. Wolfel, C. Collesi, S. Giovedi, A. Raimondi, L.W. Gong, P. Ariel, S. Paradise, E. O'Toole, R. Flavell, O. Cremona, G. Miesenbock, T.A. Ryan, P. De Camilli, A selective activity-dependent requirement for dynamin 1 in synaptic vesicle endocytosis, Science 316 (2007) 570–574.
[5] H. Cao, F. Garcia, M.A. McNiven, Differential distribution of dynamin isoforms in mammalian cells, Mol. Biol. Cell 9 (1998) 2595–2609.
[6] P.G. Noakes, D. Chin, S.S. Kim, S. Liang, W.D. Phillips, Expression and localisation of dynamin and syntaxin during neural development and neuromuscular synapse formation, J. Comp. Neurol. 410 (1999) 531–540.
[7] W.J. Jockusch, G.J. Praefcke, H.T. McMahon, L. Lagnado, Clathrin-dependent and clathrin-independent retrieval of synaptic vesicles in retinal bipolar cells, Neuron 46 (2005) 869–878.
[8] J. Zheng, S.M. Cahill, M.A. Lemmon, D. Fushman, J. Schlessinger, D. Cowburn, Identification of the binding site for acidic phospholipids on the pH domain of dynamin: implications for stimulation of GTPase activity, J. Mol. Biol. 255 (1996) 14–21.
[9] K. Salim, M.J. Bottomley, E. Querfurth, M.J. Zvelebil, I. Gout, R. Scaife, R.L. Margolis, R. Gigg, C.I. Smith, P.C. Driscoll, M.D. Waterfield, G. Panayotou, Distinct specificity in the recognition of phosphoinositides by the pleckstrin homology domains of dynamin and Bruton's tyrosine kinase, EMBO J. 15 (1996) 6241–6250.
[10] P.M. Okamoto, J.S. Herskovits, R.B. Vallee, Role of the basic, proline-rich region of dynamin in Src homology 3 domain binding and endocytosis, J. Biol. Chem. 272 (1997) 11629–11635.
[11] S. Sever, A.B. Muhlberg, S.L. Schmid, Impairment of dynamin's GAP domain stimulates receptor-mediated endocytosis, Nature 398 (1999) 481–486.
[12] R. Ramachandran, M. Surka, J.S. Chappie, D.M. Fowler, T.R. Foss, B.D. Song, S.L. Schmid, The dynamin middle domain is critical for tetramerization and higher-order self-assembly, EMBO J. 26 (2007) 559–566.
[13] E. Solomaha, F.L. Szeto, M.A. Yousef, H.C. Palfrey, Kinetics of Src homology 3 domain association with the proline-rich domain of dynamins: specificity, occlusion, and the effects of phosphorylation, J. Biol. Chem. 280 (2005) 23147–23156.
[14] H.T. McMahon, P. Wigge, C. Smith, Clathrin interacts specifically with amphiphysin and is displaced by dynamin, FEBS Lett. 413 (1997) 319–322.
[15] T. Yamashita, T. Hige, T. Takahashi, Vesicle endocytosis requires dynamin-dependent GTP hydrolysis at a fast CNS synapse, Science 307 (2005) 124–127.
[16] H. Damke, D.D. Binns, H. Ueda, S.L. Schmid, T. Baba, Dynamin GTPase domain mutants block endocytic vesicle formation at morphologically distinct stages, Mol. Biol. Cell 12 (2001) 2578–2589.
[17] A.M. van der Bliek, T.E. Redelmeier, H. Damke, E.J. Tisdale, E.M. Meyerowitz, S.L. Schmid, Mutations in human dynamin block an intermediate stage in coated vesicle formation, J. Cell Biol. 122 (1993) 553–563.
[18] A. Quan, A.B. McGeachie, D.J. Keating, E.M. van Dam, J. Rusak, N. Chau, C.S. Malladi, C. Chen, A. McCluskey, M.A. Cousin, P.J. Robinson, Myristyl trimethyl ammonium bromide and octadecyl trimethyl ammonium bromide are surface-active small molecule dynamin inhibitors that block endocytosis mediated by dynamin I or dynamin II, Mol. Pharmacol. 72 (2007) 1425–1439.
[19] M.B. Youdim, A. Hefez, B. Oppenheim, Human platelet function as a model for investigating the clinical efficacy of chlorpromazine, Br. J. Clin. Pharmacol. 12 (1981) 535–542.
[20] M. Otomo, K. Takahashi, H. Miyoshi, K. Osada, H. Nakashima, N. Yamaguchi, Some selective serotonin reuptake inhibitors inhibit dynamin I guanosine triphosphatase (GTPase), Biol. Pharm. Bull. 31 (2008) 1489–1495.
[21] B.K. Koe, A. Weissman, W.M. Welch, R.G. Browne, Sertraline, 1S,4S-N-methyl-4-(3, 4-dichlorophenyl)-1,2,3,4-tetrahydro-1-naphthylamine, a new uptake inhibitor with selectivity for serotonin, J. Pharmacol. Exp. Ther. 226 (1983) 686–700.
[22] D.P. Figgitt, K.J. McClellan, Fluvoxamine. An updated review of its use in the management of adults with anxiety disorders, Drugs 60 (2000) 925–954.
[23] W.R. Schafer, How do antidepressants work? Prospects for genetic analysis of drug mechanisms, Cell 98 (1999) 551–554.
[24] R.F. Mullins, J.M. Skeie, E.A. Malone, M.H. Kuehn, Macular and peripheral distribution of ICAM-1 in the human choriocapillaris and retina, Mol. Vis. 12 (2006) 224–235.
[25] L.H. Wang, K.G. Rothberg, R.G. Anderson, Mis-assembly of clathrin lattices on endosomes reveals a regulatory switch for coated pit formation, J. Cell Biol. 123 (1993) 1107–1117.
[26] H.H. Sitte, P. Scholze, P. Schloss, C. Pifl, E.A. Singer, Characterization of carrier-mediated efflux in human embryonic kidney 293 cells stably expressing the rat serotonin transporter: a superfusion study, J. Neurochem. 74 (2000) 1317–1324.
[27] J.S. Herskovits, C.C. Burgess, R.A. Obar, R.B. Vallee, Effects of mutant rat dynamin on endocytosis, J. Cell Biol. 122 (1993) 565–578.
[28] E.M. van Dam, W. Stoorvogel, Dynamin-dependent transferrin receptor recycling by endosome-derived clathrin-coated vesicles, Mol. Biol. Cell 13 (2002) 169–182.
[29] J. Holmgren, I. Lonnroth, J. Mansson, L. Svennerholm, Interaction of cholera toxin and membrane GM1 ganglioside of small intestine, Proc. Natl. Acad. Sci. USA 72 (1975) 2520–2524.
[30] M.Y. Zhu, G.A. Ordway, Down-regulation of norepinephrine transporters on PC12 cells by transporter inhibitors, J. Neurochem. 68 (1997) 134–141.

# Preventative Maintenance of Drainpipes in Radioisotope Facility Using Flexible Hose

Tomoko Hiroi[1)], Shinobu.Tatsunami[1, 2)], Takio Yamamoto[3)], Rie Kuwabara[1)], Hiroshi Kouyama[1)], Hiroaki Matsui[1)]

1) Institute of Radioisotope Research, St. Marianna University Graduate School of Medicine
2-16-1 Sugao, Miyamae-ku, Kawasaki, Kanagawa 216-8511, Japan
2) Unit of Medical Statistics, Faculty of Medical Education and Culture, St. Marianna University School of Medicine
2-16-1 Sugao, Miyamae-ku, Kawasaki, Kanagawa 216-8511, Japan
3) Rad Safe Technical Service Company
3-10-12 Sotokanda, Chiyoda-ku, Tokyo 101-0021, Japan

Received Aug. 21, 2009; accepted Nov. 10, 2009

**A flexible hose made of plasticized polyvinyl chloride was introduced into underground radioactive wastewater drainpipes as preventative maintenance. We completed a seamless connection spanning the longest interval between the last confluence point and the wastewater tank. Although the flexible hose is not a construction material but rather a consumable article, it is robust against the effects of temperature change and erosion by chemical substances. Moreover, it is placed in an underground steel pipe where it is protected from UV irradiation and friction. Therefore, increased hose durability is expected. In addition, the risk of damage from earthquakes or ground subsidence is negligible due to the flexibility of the hose. Compared with a full renovation of the plumbing, the economic cost is much cheaper and the construction period is much shorter. We propose the use of flexible hoses as one of the most convenient methods to prevent leakage accidents at radioisotope facilities with underground plumbing for wastewater.**

**Key words: flexible hose, maintenance, plumbing, wastewater, pipe fitting**

## 1. Introduction

Problems arising from plumbing at radioisotope facilities have been cited often in recent official incident reports issued by the Ministry of Education, Culture, Sports, Science and Technology (MEXT)[1,2)]. Although recent guidelines recommend placing water tanks and plumbing structures in a visible space[3)], some older institutions still use underground plumbing and storage tanks for radioactive wastewater[4,5)].

Earthquakes as well as construction of new buildings near radioisotope facilities will affect the underground plumbing over time. In this context, regular inspection and review of wastewater facilities such as plumbing and reservoir tanks are necessary in order to test for leakage of wastewater. If leakage is detected, much work becomes necessary[6)], such as reporting, measurements, dose evaluation and data recording. Some of this work is based on legal requirements[7)] and thus cannot be postponed or left undone.

Therefore, we performed preventative maintenance on the underground drainpipes at our radioisotope facility. We introduced a flexible hose into the steel drainpipes. Specifically, we completed a seamless connection spanning the longest interval between the last confluence point and the wastewater tank.

## 2. Project description

### 2.1 Underground plumbing at the Institute of Radioisotope Research, St. Marianna University Graduate School of Medicine

The radiation-controlled area is located on the sixth floor of

Corresponding Author: Tomoko Hiroi
Institute of Radioisotope Research, St. Marianna University Graduate School of Medicine
2-16-1 Sugao, Miyamae-ku, Kawasaki, Kanagawa 216-8511, Japan
Tel: +81-44-977-8111 (3616)
e-mail: t2hiroi@marianna-u.ac.jp

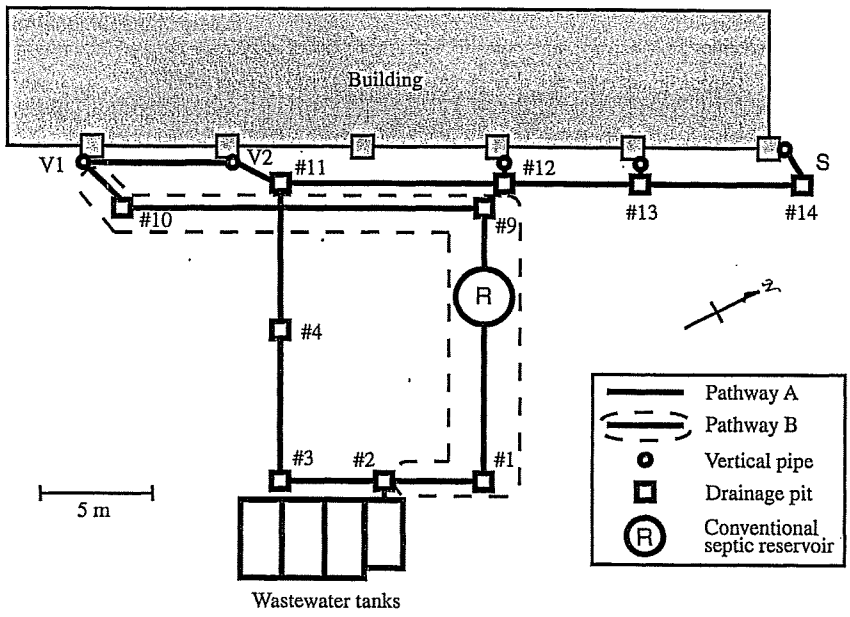


Fig. 1 Block diagram of underground plumbing.
"S", "R" and "V" indicate upstream end of water flow test for drainpipe leakage detection, a conventional septic reservoir, and position of vertical pipe, respectively.

the school building. Radioactive wastewater from the controlled area flows through five main steel pipes to a building outside. After descending from the sixth floor to the ground level, each of these pipes is connected with a drainage pit made of concrete that is buried just beneath ground level. From the five drainage pits, steel pipes lined with unplasticized polyvinyl chloride (PVC-U) follow two pathways underground (Pathway A and Pathway B) and connect to the first wastewater tank, as shown in Fig. 1.

The present renovation project consisted of three main parts:

(1) Closing Pathway B (area indicated by dotted lines in Fig. 1) including drainage pits 1, 9 and 10, as well as a conventional septic reservoir (indicated by "R" in Fig. 1). Vertical pipes 1 and 2 (indicated "V1" and "V2" in Fig.1) are connected by a new PVC-U pipe at a height of 4 m above ground level.

(2) Preventative maintenance of Pathway A via insertion of a flexible hose.

(3) Closing drainage pits 2, 3 and 4 in Pathway A.

The first step is justified only after changing the purpose of radioisotope use at our facility, namely, abrogation of animal experiment in the radiation working room. This renovation required approval from the MEXT[7], which we obtained before commencing construction for the renovation.

## 2.2 Flexible hose and fitting equipment

The primary task in the present maintenance is the introduction of the flexible hose, as shown in Fig. 2 by a photograph. The hose is made of plasticized polyvinyl chloride (PVC-P) with an outer diameter of 78.5 mm (Kanaline A, Kanaflex Co., Ltd., Roppongi, Japan). The soft body of the hose allows for flexibility and is surrounded by a PVC-U spiral (pitch: 14.3 mm) as shown in Fig. 3.

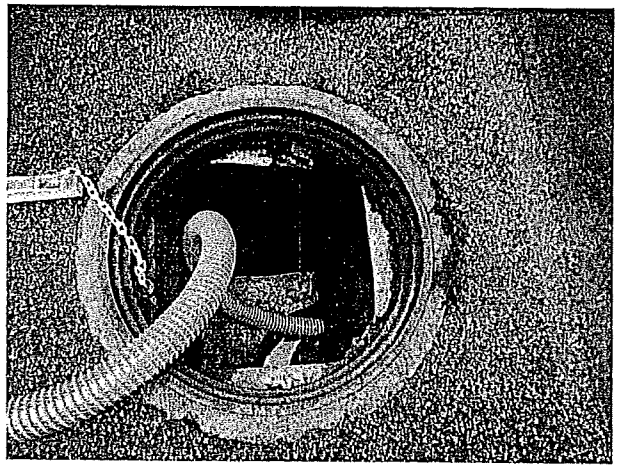

Fig. 2 Insertion of flexible hose to the plumbing.

Although the outside of the hose has a spiral structure, the inside wall is quite smooth and does not impede the flow of water. The specifications of the hose are summarized in Table 1.

Since there is a variety in diameters of opening of the concrete drainage pits, the edge of the hose was connected with a

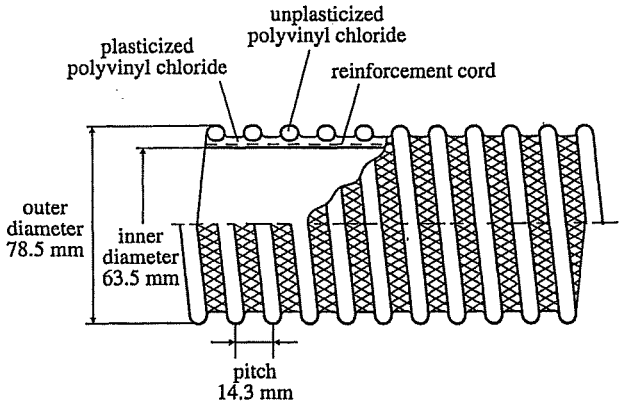


Fig. 3 Structure of flexible hose used in the present maintenance.

fitting equipment PVC-U eccentric increaser (CU INH, Aronkasei Co., Ltd., Shinagawa, Japan) as shown in Fig. 4. The pipe fitting equipment with a suitable diameter is fixed to drainage pit by using stainless steel screws and epoxy adhesive at each drainage pit.

## 3. Countermeasures and results of measurements

### 3.1 Radioactivity contamination inspections

Measurements of radioactivity were performed as part of mandated inspections for radioactivity contamination for Pathways A and B. After high-pressure washing, the surface concentration of radioactivity was measured by smear tests of the walls inside the drainage pits. The interior of the drainpipe was partly smeared except for areas that were out of reach. The radioactivity concentration was also measured in the washing drain water. Sludge was collected from the bottom of the conventional septic reservoir tank on Pathway B and was measured after drying on a small measurement plate at room temperature.

The permitted nuclides used at our institution are $^{3}H$, $^{14}C$, $^{32}P$, $^{35}S$, $^{45}Ca$, $^{51}Cr$ and $^{125}I$. Liquid scintillation counter (LSC-3500, Aloka) was used for the detection of β-rays from $^{3}H$ and $^{14}C$. A low-background gas-flow counter (LBC-472Q, Aloka) was used for the inspection of β-rays from $^{32}P$, $^{35}S$ and $^{45}Ca$. The γ-ray spectrometry was used for the evaluation of the γ-rays from $^{51}Cr$ and $^{125}I$ by using a Ge(Li) detector (G7700, Seiko EG&G Ortec).

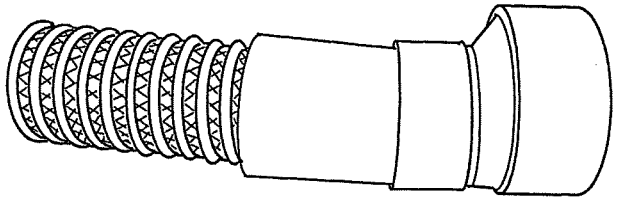

Fig. 4 Illustration of eccentric increaser; PVC-U pipe fitting.

A total of 65 pieces of filter paper from smear tests, two lots of water samples and three plates of sludge specimen were subjected to radioactivity measurements. The radioisotope contamination was lower than the detection limit for all samples collected from Pathways A and B.

### 3.2 Water flow test

The hose between the upstream and downstream ends was inspected visually with a fiberscope. Then, a leakage test was performed by letting water flow through the hose. A total of 300 L of water was passed from drainage pit 14 (point "S" in Fig. 1) at a flow rate of 16–18 L/min. The volume of the retained water in the tank was measured by using a linear scale 5–8 min after turning off the water.

The initial time lag (ITL), that is, the time interval between turning on the water and the time when the water reaches the entrance of the waste tank, was also measured. We have performed leakage inspection for the drainpipe since 2003[8]; thus, we compared the retention efficiency and ITL as measured in water flow tests before and after the present maintenance.

The time series of the observed retention efficiency is shown in Fig. 5. Two pathways were present before the renovation; thus, two series of results are shown. Before the renovation, the maximum and minimum values of water recovery for Pathway A were 109% and 94%, respectively. However, the retention efficiency has remained within the range of 100 ± 0.84% after the renovation.

The mean values of ITL before and after the renovation are summarized in Table 2. Before and after the renovation, the mean ± SD of ITL was 3.58 ± 0.88 min and 1.89 ± 0.18 min,

Table 1 Specification of hose "Kanaline A"

| Size | Weight (g/m) | Operating temperature limit (°C) | Permissible pressure (MPa) | Elongation rate at 0.4 MPa (%) | Allowable bending radius (mm) | Decompression transfomation temperature at-0.098 MPa (°C) |
|---|---|---|---|---|---|---|
| 65 | 1260 | −10~+50 | 0.490 | 15 | 270 | 60 |

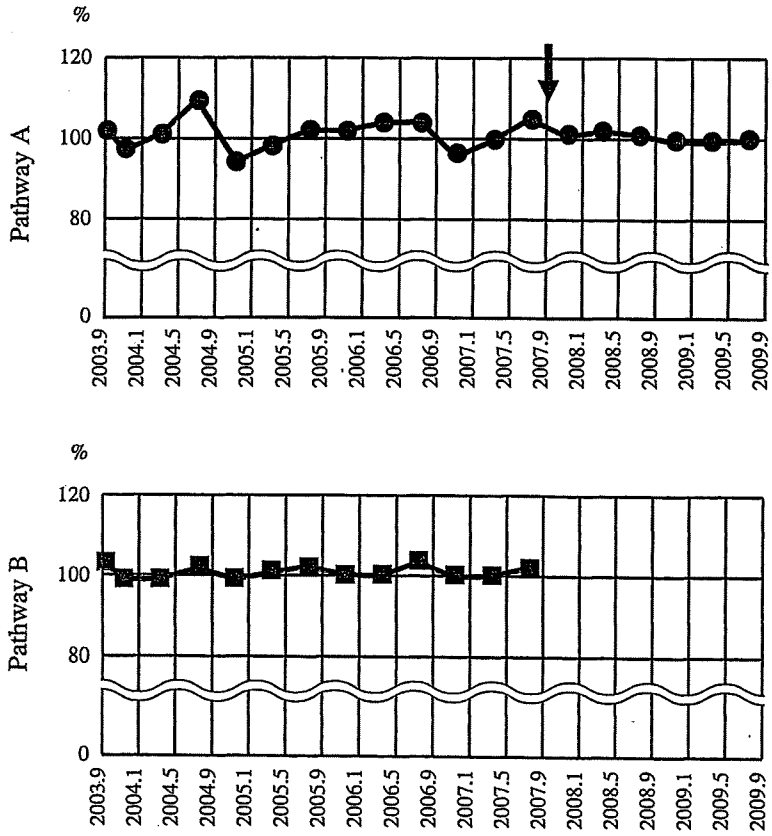


Fig. 5 Time series of retention efficiency in water flow tests since 2003 for Pathway A (top) and Pathway B (bottom). Arrow indicates time that Pathway B was closed.

Table 2 Mean ITL (min) before and after renovation

| Condition | Mean ± SD | (*n*) | Probability |
|---|---|---|---|
| Before | 3.58 ± 0.88 | (12) | $p < 0.01$ |
| After | 1.89 ± 0.18 | (6) | |

respectively. We found a statistically significant difference ($p < 0.01$) between the two means by using the *t*-test for two independent groups.

## 4. Discussion

Before the present maintenance, there were two underground pathways for the flow of wastewater, Pathways A and B, as shown in Fig. 1. The two pathways met at drainage pit 2 and then went to the wastewater tank. Since drainage pit 2 lacks a valve, it functions as a T-junction. Thus, before the closure of Pathway B, water from drainage pit 1 could flow to drainage pit 3 and water from drainage pit 3 could flow to drainage pit 1. As a result, the waiting interval after turning off the water before measuring the amount of water in the wastewater tank was subject to uncertainty in water flow tests to detect leakage from Pathway A or B. This might have resulted in the observed fluctuation of retention before the closure of Pathway B, as shown in Fig. 4. However, after closing Pathway B, the size of the fluctuation decreased. In addition, the mean of ITL showed a statistically significant decrease, as summarized in Table 2. Although these findings provide only indirect evidence of the benefits of the present maintenance, at a minimum, the results suggest that the smoothness of the present hose inside the pipes is equal to or greater than that of the steel pipe with PVC-U lining.

The flexible hose used in the present maintenance is robust against the effects of temperature change and erosion by chemical substances. Of course, its rigidity and strength are less than that of the steel drainpipe. However, the flexible hose is installed inside the steel drainpipe; thus, the risk of damage occurring due to earthquakes or ground subsidence is negligible even if a gap or a shift appeared in steel pipe junctions. Moreover, protection from UV irradiation, rain and friction beneath the ground will positively affect hose durability. Furthermore, the steel pipe is lined with a coating material, and thus there is no considerable

difference in the durability of the steel pipe with PVC-U lining and the present PVC-P hose with respect to acids or diluted alcohols resistance. The flexible hose, therefore, can serve as a suitable material for wastewater in a radioisotope facility if it is installed in a steel pipe.

At institutions using underground facilities for radioactive wastewater, a long period of time, possibly 25 years, has passed since the establishment of the controlled area. Moreover, ground subsidence[9] and earthquakes[10] frequently occur in Japan, which are necessary factors in long-term risk analysis of various facilities[11]. This means that the risk of accident due to aging drainpipes, drainage pits or fitting equipment likely has reached a considerable level.

A regular inspection procedure will detect leakage of wastewater from underground drainpipes. However, once a leakage is detected, it means an accident has already occurred. Although the present preventative maintenance requires approval from the MEXT, the preventative maintenance is much easier than taking action after an accident.

## 5. Conclusion

Renovations that include building new storage tanks and plumbing facilities will incur a large cost. In addition, such renovations may not be possible due to a lack of available space at the institution. Instead, we introduced a flexible hose into the steel drainpipes. Compared with a full renovation of the plumbing, the economic cost was lower and the construction period was much shorter. Considering its flexibility, this method will be quite advantageous for underground plumbing that will sometimes encounter ground subsidence.

## References


1. Office for Radiation Regulation, Ministry of Education, Culture, Sports, Science and Technology: Recent tendency in the governmental radiation safety management. In the textbook for the course "Radiation Safety Management", 2008, Nuclear Safety Technology Center, Chap. I (2008).
2. Ministry of Education, Culture, Sports, Science and Technology: Information on troubles, http://www.mext.go.jp/a_menu/anzenkakuho/trouble/index.html (accessed Aug 2009).
3. Central committee on protection from radiation hazards: Guidebook of Voluntary Review, Nuclear Safety Technology Center Press, Chap. 4 (1992).
4. Ministry of Education, Culture, Sports, Science and Technology: Information on troubles, http://www.mext.go.jp/b_menu/houdou/20/06/08062401.htm (accessed Aug 2009).
5. Ministry of Education, Culture, Sports, Science and Technology: Information on troubles, http://www.mext.go.jp/b_menu/houdou/21/03/1256661.htm (accessed Aug 2009).
6. Yokoyama A., Nagamura Y.: A leak accident in Drain System, The seventh Annual Convention of Japanese Society of Radiation Safety Management, Kanazawa, Abstract in Radiat. Safety Manag. 7(1), 24 (2008).
7. Japan Radioisotopes Association (Ed.): Laws on radioisotopes, Maruzen, Chap. 1 (2005).
8. Tatsunami S., Hiroi T., Masuda Y., Kuwabara R., Kouyama H., Matsui H.: Evaluation and measurement methods of radioactivity of the soil–Measurements on the campus of St. Marianna University School of Medicine, St. Marianna Med. J., 32(5), 445–451 (2004).
9. Ministry of the Environment: Directory of ground subsidence. http://www.env.go.jp/water/jiban/chinka.html (accessed Aug 2009).
10. Suzuki, Y.: About Kashiwazaki-Kariwa Nuclear Power Station after the Niigata-Chuetsu-Oki Earthquake, Japanese Journal of Health Physics, 43(1), 21–24 (2008).
11. Deck O., Verdel T., Salmon R.: Vulnerability assessment of mining subsidence hazards, Risk Anal., in press (2009).

Original Paper

Ophthalmic Research

Ophthalmic Res 2010;43:79–91
DOI: 10.1159/000247592

Received: May 20, 2008
Accepted after revision: October 10, 2008
Published online: October 15, 2009

# Transfection with *pax6* Gene of Mouse Embryonic Stem Cells and Subsequent Cell Cloning Induced Retinal Neuron Progenitors, Including Retinal Ganglion Cell-Like Cells, in vitro

Maki Kayama[a, b] Manae S. Kurokawa[b] Yuji Ueda[b] Hiroki Ueno[a]
Yuta Kumagai[a] Shummei Chiba[b] Erika Takada[b] Satoki Ueno[a]
Mamoru Tadokoro[c] Noboru Suzuki[b, d]

Departments of [a]Ophthalmology, [b]Immunology and Medicine, and [c]Pathology, St. Marianna University School of Medicine, [d]Department of Regenerative Medicine, Institute of Advanced Medical Science, St. Marianna University Graduate School of Medicine, Kawasaki, Japan

**Key Words**
Embryonic stem cell · Neuron · Differentiation · Transcription factor · Calcium flux

**Abstract**
***Objective:*** It is theoretically possible to induce various cell types, including retinal neurons, from embryonic stem cells (ESCs). *pax6* regulates early events in eye development, including the generation of retinal ganglion cells (RGCs). We previously reported the successful induction of corneal epithelial cells from ESCs transfected with the *pax6* gene. Here, we attempted to establish cloned RGC-like cells from ESCs transfected with the *pax6* gene. ***Methods:*** Undifferentiated mouse ESCs were transfected with *pax6* cDNA by electroporation, followed by selection with G418. We conducted limiting-dilution culture of *pax6*-transfected cells. We expanded the cloned *pax6*-transfected cells, which expressed nestin and musashi-1, for further characterization in culture media containing fibronectin. The cells were characterized using RT-PCR, immunostaining, electron microscopy, renal subcapsular transplantation assay and Ca imaging. ***Results:*** We obtained clonally expanding *pax6*-transfected cells, all of which were positive for six3, sonic hedgehog (shh), math5, brn3, thy1 and melanopsin, by using several ESCs. When transplanted into a mouse renal capsule, they differentiated into neurons with elongated axons, expressing βIII tubulin and neurofilament middle chain, and were free from teratoma development. Electron-microscopic examination showed neurotubules and neurofilaments in the axon-like processes of the cloned *pax6*-transfected cells. High KCl stimulation increased free Ca influx on $Ca^{2+}$ imaging. ***Conclusions:*** ESCs were applicable for the induction of retinal progenitor cells, including RGC-like cells, by transfection with the *pax6* gene and subsequent limiting-dilution culture. Cloned cell lines may be useful to analyze the requirements for retinal progenitor cell differentiation, and our study suggests the clinical application of this cell type.

Copyright © 2009 S. Karger AG, Basel

## Introduction

It has been shown that retinal progenitor cells are multipotent and retain their ability to generate different cell types such as 6 major neuronal cell types and 1 glial cell type [1]. Retinal ganglion cells (RGCs) in the eye originate from the diencephalon [2, 3] and are first induced from

KARGER
Fax +41 61 306 12 34
E-Mail karger@karger.ch
www.karger.com

© 2009 S. Karger AG, Basel
0030–3747/10/0432–0079$26.00/0

Accessible online at:
www.karger.com/ore

Dr. Noboru Suzuki, Departments of Immunology and Medicine
St. Marianna University School of Medicine
2-16-1 Sugao, Miyamae-ku, Kawasaki, Kanagawa 216-8511 (Japan)
Tel. +81 44 977 8111, ext. 3545, Fax +81 44 975 3315
E-Mail n3suzuki@marianna-u.ac.jp

retinal progenitor cells in embryonic development [3]. They elongate axons within the optic nerve, which convey important visual information to the brain. RGCs are often damaged in patients with glaucoma, leading to the apoptotic death of RGCs [4, 5] and visual impairment. The limited capacity for structural and functional repair in the retina is partly explained by the inability of the mature central nervous system to regenerate new cellular components in response to damage [6].

Embryonic stem cells (ESCs) are derived from the inner cell mass of blastocyst stage embryos and harbor self-renewing potential and multipotential. ESCs may become an unlimited source of cells suitable for such transplantation therapy. They have been shown to differentiate preferentially into multiple neural cell types [7] when cultured with medium depleted of all-*trans* retinoic acid and fetal calf serum (FCS) [8].

The paired box 6 *(pax6)* gene, containing a paired domain and a paired-type homeodomain, is one of the key transcription factors in eye development [9–11]. Indeed, *pax6* gene knockout resulted in a small-eye/eyeless phenotype in mice [12]. *pax6* gene expression is maintained throughout neuroretinal development, including RGC development [10, 13]. We thus consider that *pax6* transfection into ESCs may induce retinal neurons, including RGCs and/or their precursors.

Based on these findings, we attempted to establish cloned RGCs and/or their precursors. We first transfected ESCs with the *pax6* gene and subsequently conducted a limiting-dilution culture where culture medium was supplemented with 0.05% fibronectin. We report here the induction of retinal neuron precursors, including RGC-like cells in culture.

## Materials and Methods

*Mouse ESCs*

In this study, we used an ES cell line, E14.1, donated by Dr. Klaus Rajewsky, Cologne University (Passage No. 12–18, normal karyotype) [14]. The culture medium consisted of Dulbecco's modified Eagle's medium (DMEM), supplemented with 2 mM glutamine, 0.1 mM β-mercaptoethanol, 1 × pyruvate, and 15% FCS. Undifferentiated ESCs were maintained in the presence of mitomycin-C-treated mouse fetal fibroblasts on gelatin-coated Petri dishes in medium supplemented with 1,000 U/ml of recombinant mouse leukemia inhibitory factor (Life Technologies, Grand Island, N.Y., USA) [15]. We found that our undifferentiated ESC preparation expressed sox2, oct4 and nanog mRNA (data not shown), suggesting its undifferentiated status [16]. We conducted similar experiments with another ES cell line, R-CMT1, and obtained essentially the same results.

pax6 *cDNA Expression Vectors*

Mouse *pax6* cDNA was kindly donated by Dr. Barbara Norman (National Eye Institute, Bethesda, Md., USA). The *pax6* cDNA was ligated in a frame of green fluorescence protein (GFP) cDNA and then subcloned into pcDNA 3.1 vector (Invitrogen, Carlsbad, Calif., USA). The resultant vector expressed *pax6* + GFP fusion protein and was designated as ppax6-GFP vector. ESCs were transfected with the empty vector (GFP cDNA only) for use as a control. Although cytomegalovirus promoter allows for a strong short-term expression of transduced genes, it became silent within a few weeks after gene transfer [17]. We confirmed that *pax6* and GFP colocalized on the nuclei at days 1 and 28 of cell culture by immunostaining. Thus, it is possible that the complete silencing of *pax6* gene expression did not occur until 28 days. Transfection into undifferentiated ESCs was performed by electroporation (Bio Rad, Hercules, Calif., USA), and cells transfected with the *pax6* expression vector were selected in medium containing 100 μg/ml G418. Fourteen days after initiation of selection culture, G418-resistant cells were recovered and maintained in DMEM supplemented with 10% FCS on gelatin-coated dishes in the presence of G418.

*Limiting Dilution Culture*

Our transient transfection experiments of mouse ESCs showed that some *pax6*-transfected cells differentiate into neuron-like cells. To establish whether these cells differentiate into retinal neurons and/or their precursors, we conducted a limiting-dilution culture as previously described [18]. The growing cloned cells were transferred from 96-well plates to 24-well plates. We cultured them in medium (designated as differentiation medium) composed of DMEM: nutrient mixture F-12 (DMEM/F12) with N2 supplement (Invitrogen, Tokyo, Japan), and 0.05% fibronectin (Sigma, Tokyo, Japan) for neural induction. We repeated the transfection and limiting-dilution culture 4 times and confirmed the reproducibility.

*Reverse-Transcriptase Polymerase Chain Reaction*

Total RNA extraction, cDNA synthesis and polymerase chain reaction (PCR) amplification have been reported [14]. β-Actin was used to detect housekeeping gene expression in all reverse-transcriptase (RT)-PCRs. The sequences and annealing temperature of the primers are shown (table 1).

*Immunostaining*

Immunostaining was performed as previously described [14]. Cells cultured on a chamber slide were fixed in a mixture of methanol and acetone for 10 min at room temperature. They were blocked for 2 h in 0.2% Tween 20 and 0.2% gelatin in PBS.

They were incubated overnight with one of the following primary antibodies: anti-Pax6 (1:300; BAbCO, Evanston, Ill., USA), anti-nestin (1:400; ARP, Belmont, Mass., USA), anti-βIII tubulin (TUB) (1:400; Promega, Madison, Wisc., USA), anti-neurofilament middle chain (NFM) (1:400; Chemicon, Temecula, Calif., USA), anti-islet1 (1:200; donated by Dr. Thomas M. Jessell, Columbia University, N.Y., USA), anti-Brn3 (1:50; Santa Cruz Biotechnology, Santa Cruz, Calif., USA), anti-thy1 (1:50; Santa Cruz Biotechnology), anti-melanopsin (1:1,000; Affinity Bioreagents, Golden, Colo., USA) and anti-crx (1:1,000; kindly donated by Dr. Craft, University of Southern California) [19].

An appropriate biotin-labeled second antibody (Dako Cytomation, Kyoto, Japan) and Cy3-conjugated streptavidin (Jackson

**Table 1**

| Primer | Foward primer (5′→3′) | Reverse primer (5′→3′) | Annealing temperature, °C | PCR product, bp |
|---|---|---|---|---|
| Pax6 | aacaacctgcctatgcaacc | cttggacgggaactgacact | 54 | 206 |
| Nestin | ctaccaggagcgcgtggc | tccagagccagctggaactt | 64 | 219 |
| Musashi-1 | gagactgacgcgccccagcc | cgcctggtccatgaaagtgacg | 61 | 213 |
| TUB | tagtggagaacacagacgaga | ctgctgttcttactctggatg | 55 | 442 |
| NFM | gccgagcagaacaaggaggccatt | ctggatggtgtcctggtagctgct | 64 | 186 |
| β-Catenin | gtggaccccaagccttaggta | atggtgggtgcaggagttta | 60 | 547 |
| Shh | cctctcctgctatgctcctg | gtggcggttacaaagcaaat | 50 | 248 |
| Math5 | caggacaagaagctgtccaa | gggtctacctggagcctagc | 55 | 173 |
| Islet1 | gcagcataggcttcagcaag | atagcaggtccgcaaggtg | 55 | 365 |
| Brn3a | atgtccatgaacagcaagca | agtgcagcgacgggtactt | 45 | 216 |
| Brn3b | tctggaagcctacttcgcca | ccggttcacaatctctctga | 50 | 350 |
| Thy1 | caccaaggataactccataa | gccacacttgaccagcttgt | 55 | 266 |
| Melanopsin | tcttcatcttcagggccatc | ttctctgctgtaggccacata | 55 | 957 |
| PKC | gccatcagtaatcatgccact | ggaacccaaactatgctctt | 52 | 284 |
| Crx | agcggcgggagcggaccacattca | tggaccctggactcaggcagattg | 60 | 136 |
| Opsin | gggactgagaaagcatcgag | ccatactggcctggaactgt | 57 | 186 |
| Otx2 | gagaggacgacttttactag | ttaaaccatacctgcaccct | 55 | 185 |
| Emx1 | agcgacgttccccaggacgggct | cggttgatatggtgggaacc | 53 | 290 |
| Emx2 | ccaccttctacccctggctcatcc | gcctgcttggtagcaattctccacc | 53 | 373 |
| En1 | gtgtggcccgcctgggtctac | cgtgatatagcggtttgcctggaactc | 66 | 177 |
| En2 | gataacatcctgcggcctgag | ctgtgccatgaggtgcaccgc | 60 | 720 |
| Lim1 | atgcctgtctggggcggt | taggcctgtgaggttgag | 64 | 300 |
| HB9 | ccctgccgaccccatcaa | gccttgtcccccgaaacc | 56 | 441 |
| L-type α1C | tcgtgggtttcgtcattgtca | cctctgcactcatagagggagag | 55 | 473 |
| L-type α1D | gagcctcgattagtatagtggaatg | aggatgcagcaacagtccata | 55 | 217 |
| L-type α1F | gaagcagcagatggaagaag | tgtgtggagcgagtagagtg | 50 | 206 |
| N-type α1B | gaagtagctgaagtcagcc | cttgcgtgtcagcccctgga | 50 | 420 |
| P/Q-type α1A | gagcggctggatgacacggaacc | gagctggcgactcaccctggatgtc | 50 | 483 |
| T-type α1G | tacggaggctggagaaaa | gatgatggtggg(a/g)ttgat | 50 | 697 |
| T-type α1H | cgcagactattcacacac | gatgatggtggg(a/g)ttgat | 49 | 449 |
| T-type α1I | ggaaaagaagcgccgtaa | gatgatggtggg(a/g)ttgat | 49 | 325 |
| R-type α1E | gagactgtggtgacttttgaggacc | atagagctatggggcaccatggct | 49 | 364 |
| NMDAR 2A | gctacgggcagacagagaag | gtggttgtcatctggctcac | 57 | 257 |
| NMDAR 2B | ggctacggctacacatggat | ctgctctctccctaccatgc | 57 | 339 |
| β-Actin | gatgacgatatcgctgcgctg | gtacgaccagaggcatacagg | 55 | 440 |

Immuno Research, West Grove, Pa., USA) were used for the development of immunofluorescence. A confocal laser scanning microscope (LSM510, Carl Zeiss, Iena, Germany) was used to detect signals.

*Transplantation of Cloned* pax6*-Transfected Cells under the Renal Capsule of Mice*

We adhered to the tenets of the NIH statement for the use of Animals in Research in the following study. The subrenal capsule is suitable to obtain sufficient blood supply to the graft to promote potent cell growth. In addition, it is easier to fix cells at the transplanted site [20, 21]; therefore, we transplanted these cells under the renal capsule of mice to determine whether the cloned *pax6*-transfected cells fully differentiate into mature neurons in vivo without tumor development [20, 21]. All subsequent procedures were conducted according to the Association for Research in Vision and Ophthalmology Statement for the Use of Animals in Ophthalmic and Vision Research and received the approval of the Animal Care Facility of St. Marianna University School of Medicine.

Female C57BL/6 mice aged 6 weeks (Charles River, Kanagawa, Japan) were anesthetized with sevoflurane (Maruishi Pharmaceutical, Osaka, Japan) and were placed in a stereotaxic frame (Narishige Scientific Instrument, Tokyo, Japan).

The dorsum cavity was opened and the cloned *pax6*-transfected cells were transplanted into the renal capsule. Three groups were established; the group transplanted with cloned *pax6*-transfected cells (n = 6), the control group (PBS injection; n = 6) and the group transplanted with undifferentiated ESCs (n = 3). For the transplanted group, a single cell suspension ($2 \times 10^6$) of cloned *pax6*-transfected cells was transplanted under the capsule of the left kidney. In the control groups, either the vehicle (PBS) or un-

differentiated ESCs was similarly injected. The operations were performed using a 1-ml syringe attached to a 31-gauge needle. Fourteen days after transplantation, the kidneys were removed for analysis.

*Calcium Imaging*

Intracellular free calcium levels were evaluated using fluo-3-acetoxymethyl (AM) ester (Dojindo, Kumamoto, Japan) [14, 22, 23]. Briefly, 14 days after switching DMEM/10% FCS medium to DMEM/F12 medium with N2 supplement and fibronectin, more than 90% of the cloned *pax6*-transfected cells were Brn3 positive on immunostaining (fig. 2M). Then, the cells were transferred to glass-bottomed dishes and used for analysis. The cells were loaded with 1 μM of fluo-3-AM. Endogenous esterases converted the nonfluorescent fluo-3-AM into fluorescent fluo-3. After washing, the cells were kept in a calcium mobilization buffer containing 130 mM NaCl, 5.4 mM KCl, 1.8 mM $CaCl_2$, 0.8 mM $MgCl_2$, 5.5 mM D-glucose, and 10 mM HEPES (pH 7.3). Fluo-3 dye was excited with an argon laser at 488 nm, and fluorescence emission at λ >510 nm was captured every 5 s for 200 s.

Nomarski differential interference contrast microscopic images were recorded simultaneously to avoid focal errors. The fluo-3 fluorescence before potassium application was mostly uniform but sometimes brighter in the cells. To see the voltage-gated calcium influx, 100 mM KCl was added after recording the base emission intensity. $Ca^{2+}$ influx was induced by adding KCl with a pipette onto the cells under investigation as well as to proximal cells from 0.8 to 2 s. It has been shown under a whole-cell current clamp that the application of 100 mM KCl led to a constant membrane potential of –10 mV [14, 24].

In some experiments, lead chloride (10 μM) (Sigma), a $Ca^{2+}$ channel blocker, was added before KCl stimulation. Ionomycin (4 μM) (Molecular Probes, Eugene, Oreg., USA) was added at the end of each measurement as a positive control for $[Ca^{2+}]_i$ increase.

Addition to the bath of 0.005% saponin in 0 $Ca^{2+}$ Ringer's solution with 10 mM EGTA rapidly quenched an average of 86% of the whole cell confocal fluorescence after fluo-3 loading (n = 4), indicating predominantly cytoplasmic localization of the dye. Thapsigargin (TG) (Sigma), an irreversible inhibitor of sarcoplasmic-endoplasmic reticulum $Ca^{2+}$ ATPases, was dissolved in 0.02% ethanol. Four micromoles of TG were added at 20 min before KCl stimulation. In $Ca^{2+}$-free solution, $CaCl_2$ was removed. Nifedipine, an L-type $Ca^{2+}$ channel inhibitor, was obtained from Sigma. In all experiments, we repeated the same experiments at least 4 times.

*Statistical Analysis*

Data were averaged and expressed as means ± SEM. For comparisons between the groups the unpaired Student's t test was used, and significance was defined as $p < 0.05$.

## Results

*Induction of Cloned* pax6*-Transfected Cells*

We constructed a vector expressing *pax6* + GFP fusion protein, and introduced it into mouse ESCs. We previously found that the transfection of ESCs with the *pax6* gene differentiated not only corneal epithelial cells but also neural cells [25]. After 2 weeks' culture with G418, half of the cells developed a neuron-like configuration and the remaining cells had an epithelial cell-like configuration. In order to obtain purified neural cells, we then conducted a limiting-dilution culture (fig. 1A). *pax6*-transfected cells became membrane alkaline phosphatase negative whereas undifferentiated ESCs were alkaline phosphatase positive (fig. 1B) [26].

After limiting-dilution culture, we picked up the cloned cells expressing nestin mRNA and musashi-1 mRNA, both of which were neural stem/precursor markers (fig. 2A) [27, 28]. Cells with axon-like processes emerged when cultured in differentiation medium (fig. 1C) [29]. During the culture period of 14 days, they gradually extended axon-like processes that eventually led to the formation of neural-network-like structures (fig. 1D, E). Some of the cells had multiple axons and a fat cell body resembling authentic RGCs (fig. 1F) [30]. The *pax6*-transfected cells did not extend axon-like processes without the addition of fibronectin to culture medium (fig. 1G). The cells transfected with empty vector did not differentiate into neuron-like cells such as cells with axon-like processes (fig. 1H). They did not grow and disappeared thereafter.

To test whether cloned *pax6*-transfected cells expressed neural-cell-associated mRNA, we performed reverse-transcriptase polymerase chain reaction (RT-PCR) analyses. Cells cultured for 4 days in DMEM/F12 medium with N2 supplement and fibronectin (differentiation medium) expressed neural cell-associated mRNA, TUB [31], neurofilament middle chain (NFM) [32] and β-catenin (fig. 2A) [33].

We examined the expression of RGC-associated genes, including six3, sonic hedgehog (shh), math5, islet1, brn3a, brn3b, thy1 and melanopsin, using RT-PCR.

Islet1 is a homeodomain family transcription factor and one of the RGC markers in the earliest development process [34]. Brn3 POU domain transcription factors, brn3a, brn3b and brn3c, play essential roles in the differentiation and survival of projection neurons within RGCs [35, 36]. Thy1 plays a role in developmental milestones in the formation of the visual system [37]. Melanopsin is an opsin-like protein whose coding mRNA is found in a subset of RGCs and is proposed to be the photopigment of intrinsically photosensitive RGCs [38].

The cloned cells were simultaneously found to be positive for six3, shh, math5, islet1, brn3a, brn3b, and thy1 4 days after culture in DMEM/F12 medium with N2 sup-

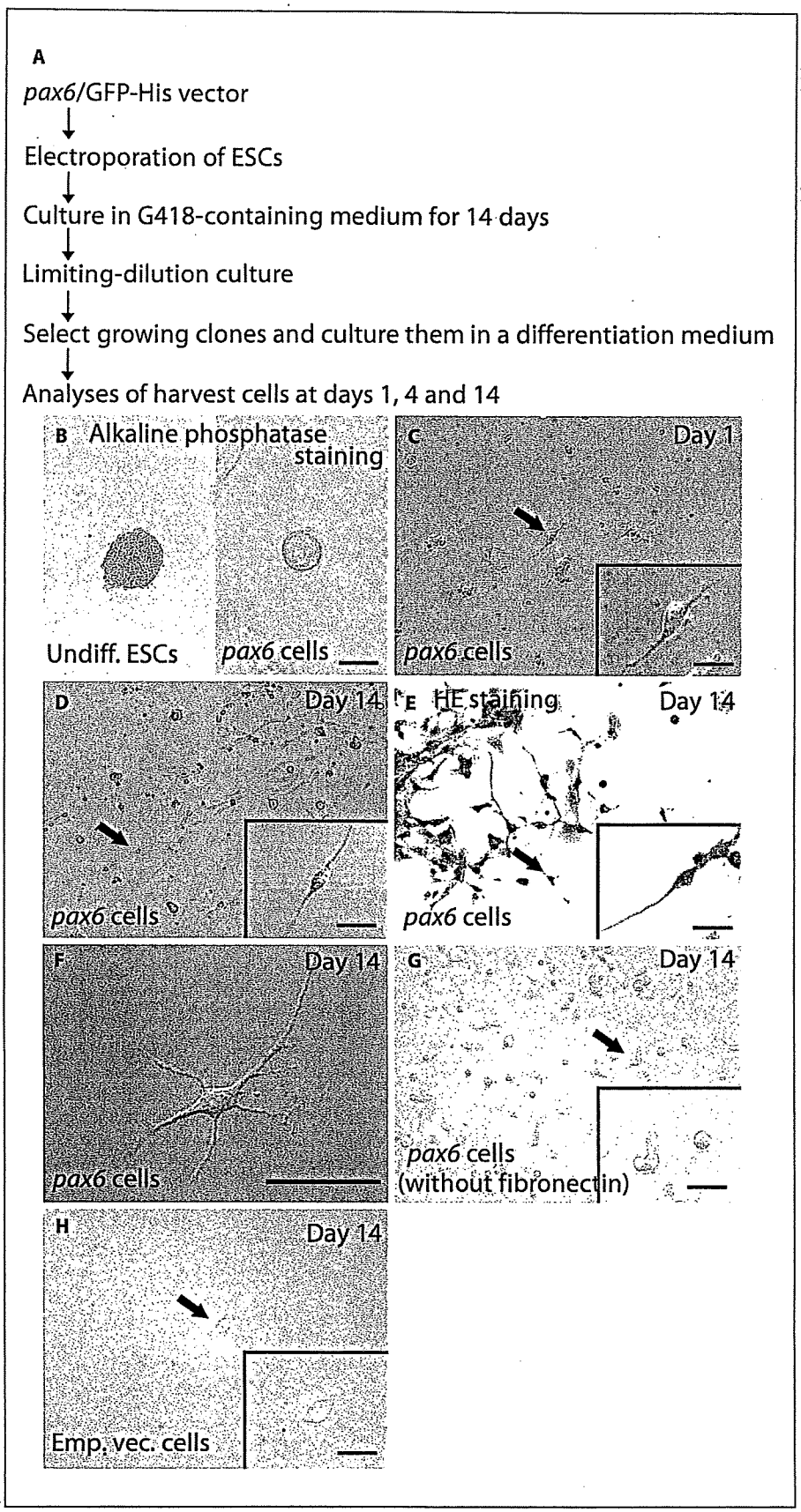


Color version available online

**Fig. 1.** Characterization of cloned *pax6*-transfected cells (*pax6* cells). Undiff. = undifferentiated. **A** Experimental protocol. *pax6* cDNA was subcloned into eukaryotic expression vector. ESCs were electrotransfected with the vector. The cells were selected by culturing in G418-containing medium for 14 days. To establish clonal cells of RGCs, limiting-dilution culture of G418-resistant cells was carried out. We picked up cloned *pax6*-transfected cells expressing nestin and musashi-1 mRNA. These cell lines were cultured in medium comprised of DMEM/F12 with N2 supplement and fibronectin (designated as differentiation medium). After sufficient expansion, cloned *pax6*-transfected cells with axon-like processes were harvested at days 1, 4 and 14 after the last passage. **B** Alkaline phosphatase staining. The *pax6*-transfected cells were negative for alkaline phosphatase. Undifferentiated ESCs were membrane alkaline phosphatase positive. **C** Inverted microscopic view of cloned *pax6*-transfected cells at day 1. **Inset:** Higher magnification of the cell indicated by an arrow. The cell had axon-like processes. **D** Inverted microscopic view of the cloned *pax6*-transfected cells at day 14. **Inset:** Higher magnification of the cell indicated by an arrow. The cell had elongated axon-like processes. **E** Hematoxylin and eosin staining of cloned *pax6*-transfected cells at day 14. They had long axon-like processes and constituted a neural network-like structure. **Inset:** Higher magnification of **E**. **F** Inverted microscopic view of cloned *pax6*-transfected cell at day 14 with multiple axon-like processes. **G** Inverted microscopic view of cloned *pax6*-transfected cells at day 14 in differentiation medium without fibronectin. **Inset:** Higher magnification of the cell indicated by an arrow. The cells did not have axon-like processes. **H** Inverted microscopic view of empty vector-transfected cells at day 14 in culture. These cells gradually disappeared. **Inset:** Higher magnification of the cell indicated by an arrow. The cell did not have axon-like processes. Bars: **B** 20 μm, **C–E, G, H**) 15 μm, (**F**) 50 μm.

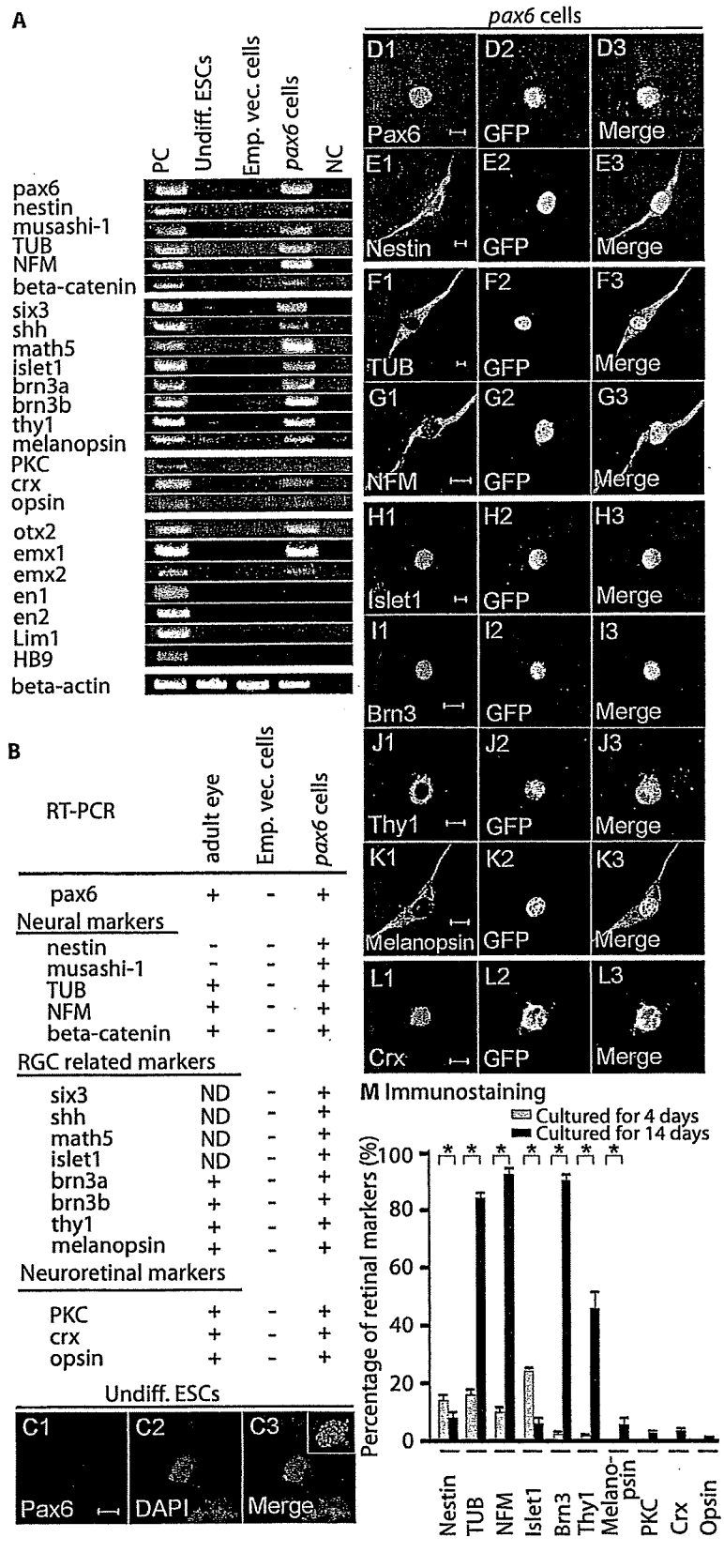


Color version available online

plement and fibronectin (fig. 2A). At the mRNA level, they were positive for bipolar cell marker, PKC [39], and photoreceptor-related markers, crx and opsin (fig. 2A) [19, 40]. The expression profile of these mRNAs was similar to that of adult mouse eye (fig. 2B).

With immunostaining, we found that 4 days after culture in differentiation medium, 14.8 ± 1.8% of the cloned *pax6*-transfected cells expressed nestin, 16.6 ± 1.8% expressed TUB, and 9.5 ± 1.2% expressed NFM (mean ± SEM, n = 3) (fig. 2M). Cells transfected with empty vector expressed neither TUB nor NFM. Overall, 24.9 ± 2.8% of the cloned *pax6*-transfected cells expressed islet1, 2.2 ± 0.01% Brn3, and 1.3 ± 0.01% thy1; however, 4 days after culture in differentiation medium, the cells did not express melanopsin, PKC, crx and opsin. Undifferentiated ESCs and cells transfected with empty vector lacked neural and RGC marker expression (summarized in fig. 2B).

We next analyzed region-specific transcription factors otx2, emx1, emx2, engrailed (en)1 and en2. In early embryogenesis, otx2, a paired homeodomain transcription factor, is found in RGCs [33] and the retinal primordia are derived from the rostral region expressing six3 [41]. emx1 and emx2 are transcription factors proposed to regulate the regionalization of the diencephalon [42]. en1 and en2 are transcription factors regulating mesencephalic regionalization [43]. The cloned cells expressed mRNA of otx2, six3, emx1 and emx2, but lacked en1 and en2 (fig. 2A). Cloned *pax6*-transfected cells lacked motoneuron-specific markers, lim1 and HB9 expression (fig. 2A).

Immunostaining demonstrated that cloned *pax6*-transfected cells expressed Pax6. Endogenous *pax6* expression of undifferentiated ESCs was very weak (fig. 2C1). Pax6 and GFP colocalized on the nucleus of cloned *pax6*-transfected cells 1 day (fig. 2D1–D3) and 28 days after culture in differentiation medium (data not shown). Fourteen days after culture in differentiation medium, the cloned *pax6*-transfected cells showed a more differentiated phenotype: 8.9 ± 1.6% of them expressed nestin, 84.3 ± 1.6% TUB, 91.8 ± 1.9% NFM, 6.4 ± 0.6% islet1, 91.8 ± 0.6% Brn3, 45.8 ± 5.5% thy1, and 7.9 ± 3.5% melanopsin (fig. 2E1–K1, M). It was suggested that in vitro culture brought about further maturation (fig. 2M, $p < 0.05$). Very small numbers of PKC- (2.0 ± 0.2%), crx- (5.8 ± 0.7%) (fig. 2L1) and opsin-positive cells (0.5 ± 0.1%) have appeared 14 days after culture in differentiation medium (fig. 2M). ESCs transfected with empty vector serving as controls did not express neural-progenitor-associated proteins and gradually disappeared in the limiting-dilution culture.

### *Transplantation of Cloned* pax6*-Transfected Cells under the Mouse Renal Capsule*

To determine whether cloned *pax6*-transfected cells fully differentiate into mature neurons without teratoma development in vivo [20], we transplanted cells which had been cultured for 4 days in DMEM/F12 medium with N2 supplement and fibronectin underneath the capsule

**Fig. 2.** Characterization of the cloned *pax6* transfected cells using RT-PCR and immunofluorescence staining. **A** RT-PCR of cloned *pax6*-transfected cells in vitro. Cloned cells were harvested and mRNA expression was examined. β-Actin mRNA served as an internal control. The positive control study (PC) used cDNA of appropriate tissues derived from fetal and adult mouse brain except the following: PC of melanopsin, PKC, crx and opsin was adult mouse retina and PC of HB9 was fetal mouse spine. Undiff. = undifferentiated; Emp. vec. cells = ESCs transfected with a vector lacking *pax6* cDNA and then were selected with G418; *pax6* cells = cloned *pax6*-transfected cells. A negative control study (NC) was conducted using double-distilled water. **B** Comparison of gene expression of cloned *pax6*-transfected cells with control vector-transfected cells and adult eye by RT-PCR. ND = Not determined. Gene expression studies were repeated at least 3 times independently. **C1–C3** Immunostaining with anti-Pax6 antibody of the undifferentiated ESCs. **C1** Immunostaining with anti-Pax6 antibody. **C2** DAPI was used for nuclear staining. **C3** Merged image. Endogenous expression of Pax6 in the undifferentiated ESCs was extremely weak. **Inset:** Merged image of undifferentiated ESCl colony stained with anti-Pax6 antibody (lower magnification). **D1–K3** Immunofluorescence characterization of cloned *pax6*-transfected cells. **D1** Immunostaining with anti-Pax6 antibody. **D2** GFP. **D3** Merged image. Confocal microscopic analysis indicated that cloned *pax6*-transfected cell expressed Pax6 and GFP in the nucleus, suggesting the expression of the Pax6/GFP fusion protein in the nucleus. **E1** Immunostaining with anti-nestin antibody. **E2** GFP. **E3** Merged image. The GFP-positive nucleus was surrounded by nestin-positive axons. **F1** Immunostaining with anti-TUB antibody. **F2** GFP. **F3** Merged image. **G1** Immunostaining with anti-NFM antibody. **G2** GFP. **G3** Merged image. **H1** Immunostaining with anti-islet1 antibody. **H2** GFP. **H3** Merged image. A GFP-positive nucleus overlaid islet1 immunostaining. **I1** Immunostaining with anti-Brn3 antibody. **I2** GFP. **I3** Merged image. A GFP-positive nucleus overlaid Brn3 immunostaining. **J1** Immunostaining with anti-thy1 antibody. **J2** GFP. **J3** Merged image. The cell expressed thy1 on the cell membrane, whose nucleus was GFP positive. **K1** Immunostaining with anti-melanopsin antibody. **K2** GFP. **K3** Merged image. Melanopsin immunoreactivity was located at soma and dendritic processes of cloned *pax6*-transfected cells. **L1** Immunostaining with anti-crx antibody. **L2** GFP. **L3** Merged image. A GFP-positive nucleus overlaid crx immunostaining. **M** RGC-related marker expression of 6 cloned *pax6*-transfected cell lines at days 4 and 14 judged by immunostaining. Data are the means ± SEM of 3 independent experiments. * $p < 0.05$ (unpaired Student's t test). Bars: **C1**, **D1**, **E1**, **F1**, **G1**, **H1**, **I1**, **J1**, **K1** and **L1** 10 μm.

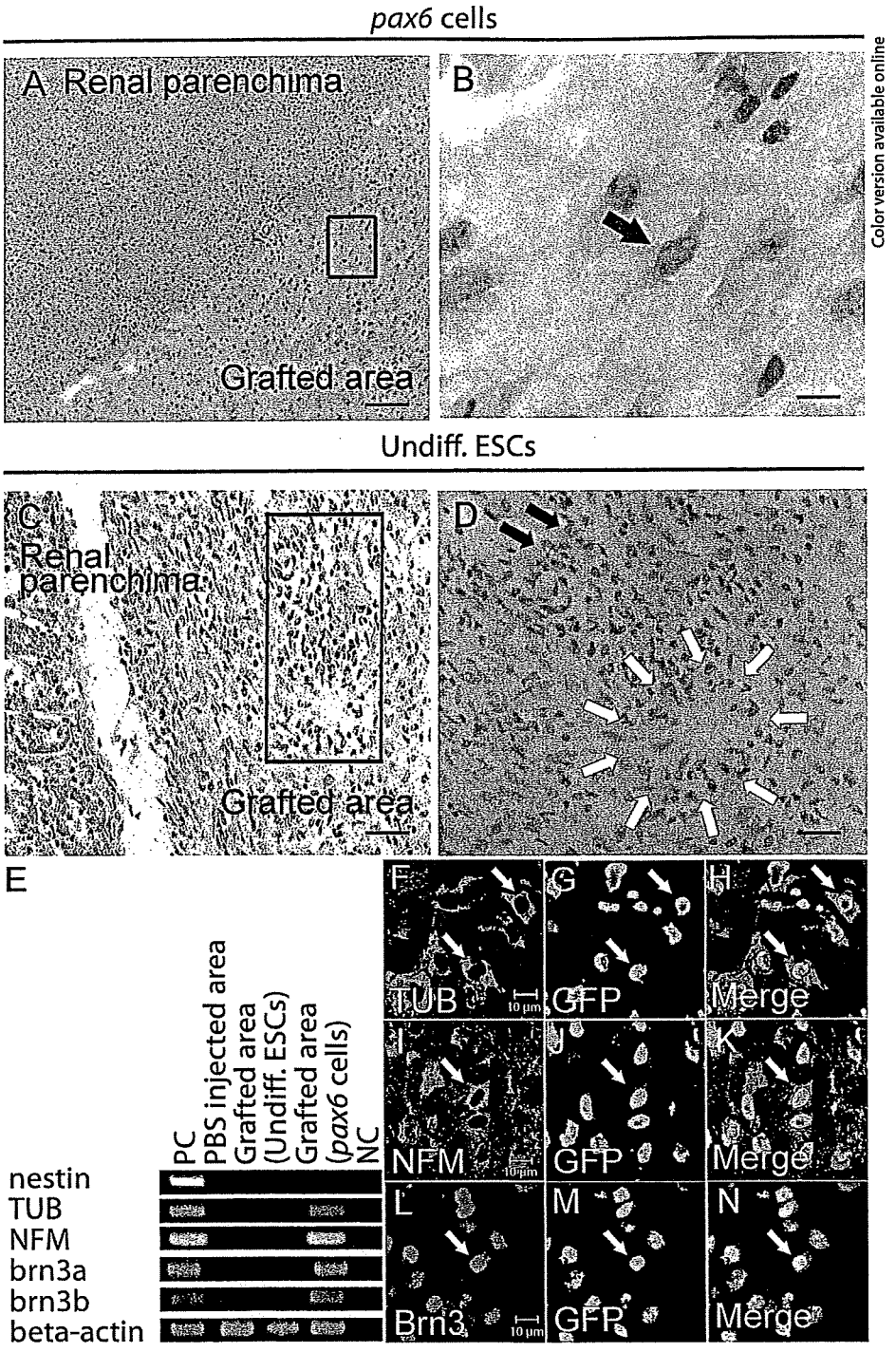


Color version available online

**Fig. 3.** Histological analyses of cloned *pax6*-transfected cells (*pax6* cells) in mouse kidney after transplantation under the renal capsule. Transplantation was performed to determine whether cloned *pax6*-transfected cells maturated fully in vivo and whether they developed teratoma in vivo. A single cell suspension of cloned *pax6*-transfected cells was used as a graft for transplantation. As a control cell, we used undifferentiated ESCs (undiff. ESCs). **A** HE staining of the boundary between the renal parenchyma and the grafted area (*pax6* cells) at day 14. **B** Higher magnification of frame area in **A**. The grafted cells had axon-like processes under the mouse renal capsule (closed arrow). We did not find teratoma development or tumor formation of other cell types in the same experiments repeated 6 times. **C** HE staining of the boundary between the renal parenchyma and the grafted area (control cell graft; undifferentiated ESCs) at day 14. **D** Higher magnification of the framed area in **C**. The grafted cells formed tumors where doctoral structure (open arrows) and pigmented cells (closed arrows) were found. We hardly found cells with axon-like processes at the grafted site. **E** RT-PCR of transplanted tissue. The expression of neuron-associated mRNA was examined. 'PBS injected area': injection area of PBS under the renal capsule of mice; grafted area (Undiff. ESCs): grafted area of undifferentiated ESCs under the renal capsule of mice; grafted area (*pax6* cells): grafted area of cloned *pax6*-transfected cells under the renal capsule of mice. The positive control study (PC) used cDNA of appropriate tissues derived from fetal and adult mouse brain. The negative control study (NC) was conducted using double-distilled water. β-Actin mRNA served as an internal control. Grafted area of *pax6*-transfected cells expressed TUB and NFM, but not nestin. brn3a mRNA and brn3b mRNA were expressed in the grafted area. Gene expression studies were repeated at least 3 times independently. **F** Immunostaining with anti-TUB antibody (open arrows). **G** GFP (open arrows). **H** Merged image. GFP-positive nuclei of grafted cells were TUB positive (open arrows). **I** Immunostaining with anti-NFM antibody (an open arrow). **J** GFP (an open arrow). **K** Merged image. GFP-positive nuclei of the grafted cells were surrounded by NFM-positive cytoplasm and axons (open arrow). **L** Immunostaining with anti-Brn3 antibody (open arrow). **M** GFP (open arrow). **N** Merged image. GFP-positive nuclei of the grafted cells overlaid Brn3 immunostaining (an open arrow). Bars: **A**, **C** 100 μm, **B**, **F**, **I**, **L** 10 μm, **D** 50 μm.

of the left kidney. Fourteen days after transplantation, the cells had grown slightly and formed a boundary between the renal parenchyma and the grafted area (fig. 3A). The transplanted cloned *pax6*-transfected cells were free from tumor development. With higher magnification, we found that neuron-like cells had accumulated in the grafted area (closed arrow in fig. 3B).

We next examined mRNA expression of grafted cells 14 days after transplantation (fig. 3E). These cells were positive for neural cell markers, TUB and NFM and RGC markers, including brn3a and brn3b, but negative for nestin.

Confocal analysis revealed that GFP-positive cloned *pax6*-transfected cells expressed TUB and NFM, suggesting maturation of the grafted cells into neurons in vivo (open arrows in fig. 3F–K). They were positive for Brn3 protein expression (open arrows in fig. 3L–N). In control experiments using undifferentiated ES cells, they formed a tumor at the grafted site. Furthermore, no cells with axon-like processes were found at the grafted site (fig. 3C, D).

To confirm our findings, we performed an electron-microscopic examination of the grafted cells (fig. 4). Cloned *pax6*-transfected cells elongated axon-like processes (fig. 4 inset). Around the boundary of the axon-like processes and cytoplasm, cloned *pax6*-transfected cells had characteristic neurotubules 24.7 nm in diameter (closed arrowheads in fig. 4) and neurofilaments 9.9 nm in diameter (open arrows in fig. 4), both of which are major cytoskeletal components of neurons, confirming that cloned *pax6*-transfected cells differentiated into neurons [44, 45].

*Calcium Imaging of Cloned* pax6*-Transfected Cells*

Voltage-gated $Ca^{2+}$ channels are composed of multiple subunits and regulate $Ca^{2+}$ influx [46]. It has been reported that RGC yielded the expression of $Ca^{2+}$ channel subtypes, L, N, P/Q, and T [47]. Most inner retinal neurons have glutamate receptors, and RGCs express N-methyl-D-aspartic acid (NMDA) receptors [48]. We found by RT-PCR that L, N, P/Q, and T subtypes of $Ca^{2+}$ channels were expressed in cloned *pax6*-transfected cells (fig. 5A). NMDA receptors 2A and 2B were also expressed (fig. 5A).

A $Ca^{2+}$-sensitive fluorescent probe, fluo-3-AM, and a scanning confocal microscope were then used to detect any changes in intracellular $Ca^{2+}$ concentrations. The basal fluorescence of the cloned *pax6*-transfected cells was moderate and was almost homogeneous, except for the nucleus, before KCl stimulation (fig. 5B).

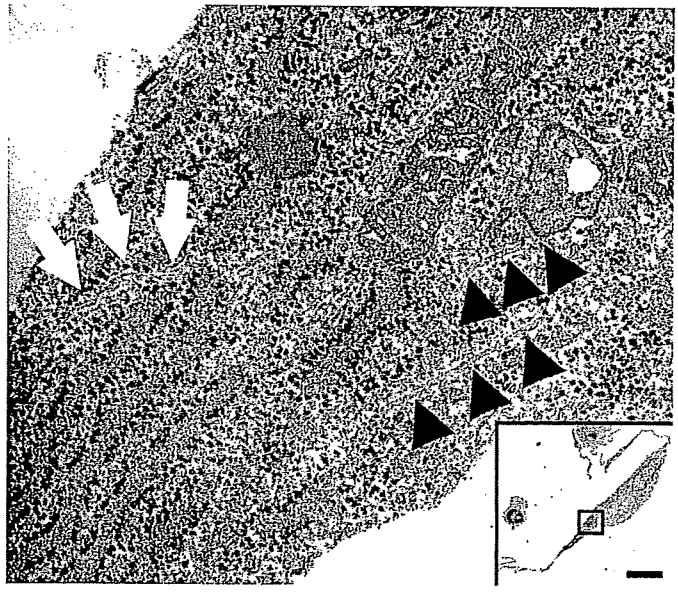

**Fig. 4.** Electron-microscopic examination of cloned *pax6*-transfected cells transplanted under the mouse renal capsule. Electron-microscopic analysis of cloned *pax6*-transfected cells transplanted under the mouse renal capsule at day 14 was conducted with high power magnification (×80,000). We found neurotubules (closed arrowheads) and neurofilament (open arrows) around the boundary between the axon-like process and the cytoplasm of the grafted cloned *pax6*-transfected cells. **Inset:** Low power image (×7,200). Bar: 10 μm.

The cells were examined again after applying a small amount of 100 mM KCl solution with a micropipette. It has been shown that application of high concentrations of KCl leads to depolarization when measured under intracellular recording [22]. The resulting fluorescence of fluo-3 increased (fig. 5C and open arrowhead in fig. 5E). The increase in $[Ca^{2+}]_i$ upon KCl stimulation showed a characteristic and easily reproducible pattern. At the end, the calcium ionophore Ionomycin was introduced as a positive control for $Ca^{2+}$ influx (fig. 5D, and closed arrowhead in fig. 5E). The depletion of extracellular calcium from the cells markedly reduced the fluorescence intensity (fig. 5F); thus, extracellular $Ca^{2+}$ was needed to elicit an increase in $[Ca^{2+}]_i$ upon stimulation of this type of cell. A similar dependency of extracellular $Ca^{2+}$ on an increase in $[Ca^{2+}]_i$ was reported in forskolin-induced $Ca^{2+}$ signals in rat olfactory receptor neurons [49].

Lead chloride is a well-known environmental neurotoxicant that blocks the function of voltage-dependent $Ca^{2+}$ channels. Treatment of cloned *pax6*-transfected cells with lead chloride inhibited the increase in $[Ca^{2+}]_i$ (fig. 5G).

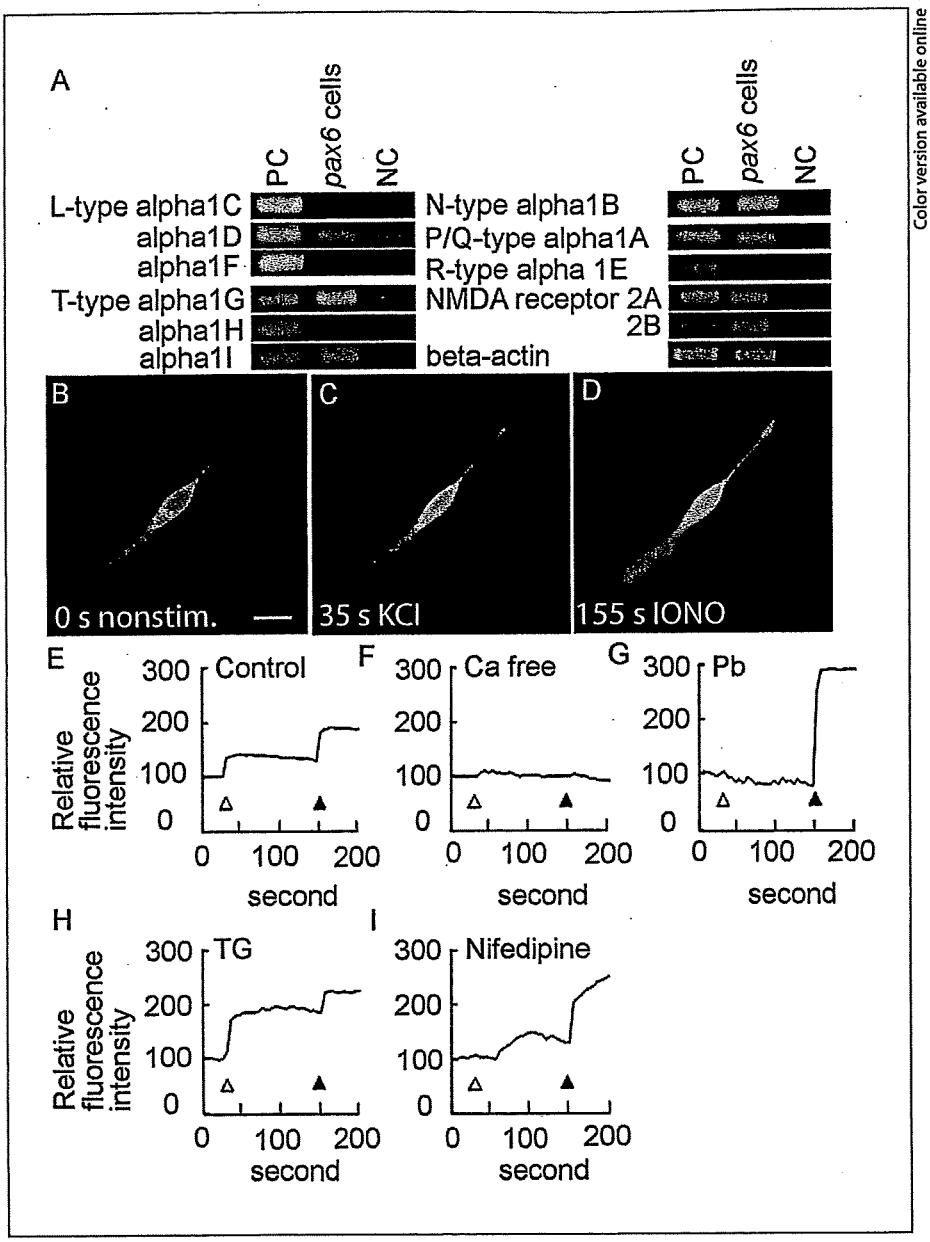


**Fig. 5.** Free Ca mobilization of cloned *pax6*-transfected cells (*pax6* cells). **A** $Ca^{2+}$ channel mRNA expression by RT-PCR. mRNA expression of $Ca^{2+}$ channel subtypes, L, N, P/Q and T and NMDA receptor subtypes, 2A and 2B, in cloned *pax6*-transfected cells were examined. β-actin mRNA served as an internal control. The positive control study (PC) used cDNA of appropriate tissues derived from adult mouse brain except for the following: the PC of α1C was cardiac muscle and that of α1D, NMDA receptors, 2A and 2B were retina. A negative control study (NC) was conducted using double-distilled water. Gene expression studies were repeated at least 4 times independently. **B–D** Cloned *pax6*-transfected cells were loaded with fluo-3-AM to detect any change of intracellular $Ca^{2+}$ concentrations after high KCl stimulation. **B** A confocal image of the representative cell without any inhibitor just before stimulation (nonstim.) at 0 s. The basal fluorescence was moderate and nearly homogeneous except for the nucleus before KCl stimulation. Bar: 10 μm. **C** Fluorescence image of the representative cell with KCl stimulation at 35 s. After stimulation with KCl, the cell elicited increased fluorescence intensity. **D** Fluorescence image of a representative cell with calcium ionophore, ionomycin (IONO, 4 μM) stimulation at 155 s as a positive control for $Ca^{2+}$ entry. 0, 35 and 155 s represent time after initiation of confocal microscopic analyses (please refer to **E–I**, horizontal axis). **E** In the absence of inhibitor (control), the cells were stimulated with the introduction of 100 mM KCl (open arrowhead), and then with ionomycin (closed arrowhead). Fluorescence intensity of more than 10 cells was measured, and relative fluorescence intensity of a representative cell was depicted. **F** Cells were stimulated similarly without $Ca^{2+}$ (in the Ca-free solution). **G** Lead chloride (Pb) 10 μM was added 20 min before KCl stimulation. **H** TG was added 20 min before KCl stimulation. **I** Nifedipine 3 μM was added 20 min before KCl stimulation.

To confirm whether the release of $Ca^{2+}$ from intracellular stores of $Ca^{2+}$ is involved in the KCl-stimulated increase in $[Ca^{2+}]_i$, we examined the effects of thapsigargin (TG), an irreversible inhibitor of sarcoplasmic-endoplasmic reticulum $Ca^{2+}$-ATPases, on $[Ca^{2+}]_i$ [50]. TG treatment had no reproducible effects on the increase in $[Ca^{2+}]_i$ upon KCl stimulation (fig. 5H). Our results indicate that the KCl-stimulated intracellular $Ca^{2+}$ increase was mainly due to the influx of $Ca^{2+}$ via $Ca^{2+}$ channels and marginally to the release of $Ca^{2+}$ from intracellular stores in cloned *pax6*-transfected cells.

Nifedipine modestly suppressed the increase in $[Ca^{2+}]_i$ (fig. 5I). It is possible that several different types of $Ca^{2+}$ channels cooperate simultaneously to induce the increase in $[Ca^{2+}]_i$ in these cloned cells.

## Discussion

In this study, we successfully induced retinal neuron progenitors, including RGC-like cells, from mouse ESCs by *pax6* gene transfection. The cells were stable for a long period of time with the expression of several RGC-related markers and maintained their characteristics as retinal neuron progenitors, including RGC-like cells for at least 20 passages, even though the expression levels of GFP gradually weakened with passaging. When we repeated the experiment, we always succeeded in establishing cloned *pax6*-transfected cells. Our present study suggested the following: *pax6*-transfected cells retained a moderate proliferative potential for a certain period. They eventually lost neural progenitor markers after long-term passaging, probably due to maturation. As mentioned, *pax6*-transfected cells as a whole contained cells in various stages of the differentiation pathway of retinal neurons. For example, cells of early passages included those with higher proliferative potential and the majority shared their characteristics with neural (and/or retinal neuron) progenitor cells. In contrast, cells with higher passage numbers included small numbers of proliferating cells (thus the majority was dormant) and the majority differentiated to some extent to more mature retinal neurons.

We previously reported that transfection of the *pax6* gene induces ESCs to differentiate into corneal epithelial cells [25]. At that time we found that the *pax6* gene induced ES cell differentiation in two cell lineages, neural cells and epithelial cells. It is possible that simple *pax6* gene transfection by itself brings about differentiation of ESCs into the stage of 'theoretical neuro-epithelial lineage', i.e. cells capable of differentiating into neural and epithelial cells. Subsequent culture conditions, including depletion of FCS, addition of fibronectin, addition of N2 supplement and so on [51], largely affect the resultant cell fate commitment of *pax6*-transfected cells.

Different extrinsic factors are known to control retinal cell fate specification, e.g. fibronectin is part of the extracellular matrix in the central nervous system and is one of the most commonly used substrates for neuronal cell cultures providing adequate support for cell growth [52]. Murashov et al. [51] studied the requirement of fibronectin for neural differentiation of mouse ESCs. Mouse ESCs were apparently well differentiated when fibronectin was supplemented to the culture medium [51]. Based on their observations, we supplemented fibronectin into culture medium for neural cell induction. Fibronectin may be important for differentiating ESCs into retinal neuron precursors, including RGC-like cells.

RGCs are first induced from retinal progenitor cells in embryonic development [3]; therefore, it is important to clarify whether cloned *pax6*-transfected cells share characteristics with retinal progenitor cells, which differentiate into all retinal cell types, including bipolar cells, photoreceptors and Muller glial cells [13]. We found that the cells consistently expressed mRNA of RGC-related markers, islet1, brn3a, brn3b, thy1 and melanopsin (fig. 2A, H1–K1). Melanopsin-positive cells comprise only 5% of RGC populations in vivo [38]. Among our 6 established cloned cell lines, we found that 7.9% of cloned *pax6*-transfected cells expressed melanopsin by immunostaining, almost compatible with the in vivo findings [38].

Occasionally, a few cell lines expressed PKC, crx and opsin protein 14 days after initiation of cell culture in differentiation medium. Muller glial-cell-related markers glial fibrillary acidic protein (GFAP) and glutamine synthase (GS) [53, 54] were not expressed at all on cloned *pax6*-transfected cells. The possibility exists that cloned *pax6*-transfected cells have potential to further differentiate into more mature retinal neurons, and that exogenous growth factors and chemokines may be required for their maturation in vitro. We are therefore conducting experiments to clarify this issue.

Math5 suppresses the production of other retinal cell types and promotes RGC formation [55, 56]. It is possible that *pax6* may induce or positively affect Math5 expression and/or functions. It has been shown that the production of RGCs is in part regulated by inhibitory factors secreted by RGCs themselves. Shh is secreted from differentiated RGCs and, through feedback mechanisms, regulates retinal precursor cell proliferation and RGC

production [57]; thus we need to study whether Shh regulates *pax6* gene expression in the developing retina in the near future [58, 59].

Expression of region-specific transcription factors clarified the properties of cloned *pax6*-transfected cells. The cells expressed diencephalon-associated markers, including otx2, six3, emx1 and emx2 (fig. 2A), consistent with authentic RGCs.

We found that cloned *pax6*-transfected cells exhibited a rapid increase in intracellular $Ca^{2+}$ in response to KCl stimulation, and that the intracellular $Ca^{2+}$ increase was mainly due to calcium influx via $Ca^{2+}$ channels and marginally due to the release of $Ca^{2+}$ from intracellular stores in cloned *pax6*-transfected cells. We previously reported a similar intracellular $Ca^{2+}$ increase in neurons induced from mouse ESCs [22]. We found that cloned *pax6*-transfected cells expressed NMDA receptors by RT-PCR (fig. 5A). Detailed functional study of glutamate and NMDA receptors are ongoing in our laboratory using several cloned *pax6*-transfected cell lines.

Electron microscopic examination disclosed the appearance of neurotubules and neurofilament in cloned *pax6*-transfected cells in vivo, suggesting their neuronal differentiation. Using cell clones, we are planning to study the differentiation requirements of retinal progenitors/RGC precursors to fully mature RGCs.

Taken together, we report here that cloned *pax6*-transfected cells include cells of retinal neuron progenitors, including RGC-like cells.

## References


1 Trimarchi JM, Stadler MB, Cepko CL: Individual retinal progenitor cells display extensive heterogeneity of gene expression. PLoS ONE 2008;13:e1588.
2 Kobayashi M, Toyama R, Takeda H, Dawid IB, Kawakami K: Overexpression of the forebrain-specific homeobox gene six3 induces forebrain enlargement in zebrafish. Development 1998;125:2973–2983.
3 Marquardt T, Gruss P: Generating neuronal diversity in the retina: one for nearly all. Trends Neurosci 2002;25:32–38.
4 De Marco N, Buono M, Troise F, Diez-Roux G: Optineurin increases cell survival and translocates to the nucleus in a Rab8-dependent manner upon an apoptotic stimulus. J Biol Chem 2006;281:16147–16156.
5 Quigley HA: Neuronal death in glaucoma. Prog Retin Eye Res 1999;18:39–57.
6 Cao Q, Benton RL, Whittemore SR: Stem cell repair of central nervous system injury. J Neurosci Res 2002;68:501–510.
7 Tropepe V, Hitoshi S, Sirard C, Mak TW, Rossant J, van der Kooy D: Direct neural fate specification from embryonic stem cells: a primitive mammalian neural stem cell stage acquired through a default mechanism. Neuron 2001;30:65–78.
8 Watanabe K, Kamiya D, Nishihyama A, Katayama T, Nozaki S, Kawasaki H, Watanabe Y, Mizuseki K, Sasai Y: Directed differentiation of telencephalic precursors from embryonic stem cells. Nat Neurosci 2005;8:288–296.
9 Chow RL, Lang RA: Early eye development in vertebrates. Annu Rev Cell Dev Biol 2001; 17:255–296.
10 Davis-Silberman N, Kalich T, Oron-Karni V, Marquardt T, Kroeber M, Tamm ER, Ashery-Padan R: Genetic dissection of Pax6 dosage requirements in the developing mouse eye. Hum Mol Genet 2005;14:2265–2276.
11 Marquardt T, Ashery-Padan R, Andrejewski N, Scardigli R, Giullemot F, Gruss P: Pax6 is required for the multipotent state of retinal progenitor cells. Cell 2001;105:43–55.
12 Hill RE, Favor J, Hogan BL, Ton VC, Saunders GF, Hanson IM, Prosser J, Jordan T, Hastie ND, van Heyningen V: Mouse small eye results from mutations in a paired-like homeobox-containing gene. Nature 1991; 354:522–525.
13 Philips GT, Stair CN, Young Lee H, Wroblewski E, Berberoglu MH, Brown NL, Mastick GS: Precocious retinal neurons: Pax6 controls timing of differentiation and determination of cell type. Dev Biol 2005;279: 308–321.
14 Hamada M, Yoshikawa H, Ueda Y, Kurokawa MS, Watanabe K, Sakakibara M, Tadokoro M, Akashi K, Aoki H, Suzuki N: Introduction of the MASH1 gene into mouse embryonic stem cells leads to differentiation of motoneuron precursors lacking Nogo receptor expression that can be applicable for transplantation to spinal cord injury. Neurobiol Dis 2006;22:509–522.
15 Chiba S, Iwasaki Y, Sekino H, Suzuki N: Transplantation of motoneuron-enriched neural cells derived from mouse embryonic stem cells improves motor function of hemiplegic mice. Cell Transplant 2003;12:457–468.
16 Rodda DJ, Chew JL, Lim LH, Loh YH, Wang B, Ng HH, Robson P: Transcriptional regulation of nanog by OCT4 and SOX2. J Biol Chem 2005;280:24731–24737.
17 Smith JR, Maguire S, Davis LA, Alexander M, Yang F, Chandran S, French-Constant C, Pedersen RA: Robust, persistent transgene expression in human embryonic stem cells is achieved with AAVS1-targeted integration. Stem Cells 2008;26:496–504.
18 Funderburgh ML, Du Y, Mann MM, SundarRaj N, Funderburgh JL: PAX6 expression identifies progenitor cells for corneal keratocytes. FASEB J 2005;19:1371–1373.
19 Bibb LC, Holt JK, Tarttelin EE, Hodges MD, Gregory-Evans K, Rutherford A, Lucas RJ, Sowden JC, Gregory-Evans CY: Temporal and spatial expression patterns of the crx transcription factor and its downstream targets. Critical differences during human and mouse eye development. Hum Mol Genet 2001;10:1571–1579.
20 Hori J, Ng TF, Shatos M, Klassen H, Streilein JW, Young MJ: Neural progenitor cells lack immunogenicity and resist destruction as allografts. Stem cells 2003;21:405–416.
21 Kroon E, Martinson LA, Kadoya K, Bang AG, Kelly OG, Eliazer S, Young H, Richardson M, Smart NG, Cunningham J, Agulnick AD, D'Amour KA, Carpenter MK, Baetge EE: Pancreatic endoderm derived from human embryonic stem cells generates glucose-responsive insulin-secreting cells in vivo. Nat Biotechnol 2008;26:443–452.
22 Ide M, Ueda Y, Watanabe K, Kurokawa MS, Yoshikawa H, Sakakibara M, Hashimoto T, Suzuki N: Characterization of intracellular free $Ca^{2+}$ movements in neural progenitor cells derived from ES cells transfected with MASH1 transcription factor gene. Inflamm Regen 2005;25:452–460.